frontiers in Marine Science

ORIGINAL RESEARCH
published: 23 November 2021
doi: 10.3389/fmars.2021.745304

Air-Sea CO_2 Exchange in the Strait of Gibraltar

*David Curbelo-Hernández, J. Magdalena Santana-Casiano, Aridane González González and Melchor González-Dávila**

Instituto de Oceanografía y Cambio Global (IOCAG), Universidad de Las Palmas de Gran Canaria (ULPGC), Las Palmas de Gran Canaria, Spain

The seasonal and spatial variability of the CO_2 system and air-sea fluxes were studied in surface waters of the Strait of Gibraltar between February 2019 and March 2021. High-resolution data was collected by a surface ocean observation platform aboard a volunteer observing ship. The CO_2 system was strongly influenced by temperature and salinity fluctuations forced by the seasonal and spatial variability in the depth of the Atlantic–Mediterranean Interface layer and by the tidal and wind-induced upwelling. The changes in seawater CO_2 fugacity ($fCO_{2,sw}$) and fluxes were mainly driven by temperature despite the significant influence of non-thermal processes in the southernmost part. The thermal to non-thermal effect ratio (T/B) reached maximum values in the northern section (>1.8) and minimum values in the southern section (<1.30). The $fCO_{2,sw}$ increased with temperature by 9.02 ± 1.99 μatm °C^{-1} (r^2 = 0.86 and ρ = 0.93) and 4.51 ± 1.66 μatm °C^{-1} (r^2 = 0.48 and ρ = 0.69) in the northern and southern sections, respectively. The annual cycle of total inorganic carbon normalized to a constant salinity of 36.7 (NC_T) was assessed. Net community production processes described 93.5–95.6% of the total NC_T change, while air-sea exchange and horizontal and vertical advection accounted for <4.6%. The $fCO_{2,sw}$ in the Strait of Gibraltar since 1999 has been fitted to an equation with an interannual trend of 2.35 ± 0.06 μatm year^{-1} and a standard error of estimate of ±12.8 μatm. The seasonality of the air-sea CO_2 fluxes reported the behavior as a strong CO_2 sink during the cold months and as a weak CO_2 source during the warm months. Both the northern and the southern sections acted as a net CO_2 sink of −0.82 and −1.01 mol C m^{-2} year^{-1}, respectively. The calculated average CO_2 flux for the entire area was −7.12 Gg CO_2 year^{-1} (−1.94 Gg C year^{-1}).

Keywords: air-sea CO_2 fluxes, CO_2 system, VOS lines, seasonal variability, Strait of Gibraltar

OPEN ACCESS

Edited by:
Alessandro Bergamasco, Institute of Marine Science, National Research Council (CNR), Italy

Reviewed by:
Iole Orselli, Federal University of Rio Grande, Brazil
Liang Xue, First Institute of Oceanography, Ministry of Natural Resources, China

***Correspondence:**
Melchor González-Dávila
melchor.gonzalez@ulpgc.es

Specialty section:
This article was submitted to Marine Biogeochemistry, a section of the journal Frontiers in Marine Science

Received: *21 July 2021*
Accepted: *26 October 2021*
Published: *23 November 2021*

Citation:
Curbelo-Hernández D, Santana-Casiano JM, González AG and González-Dávila M (2021) Air-Sea CO_2 Exchange in the Strait of Gibraltar. Front. Mar. Sci. 8:745304. doi: 10.3389/fmars.2021.745304

INTRODUCTION

Coastal and transition to open-ocean areas are biogeochemically active regions which play a key role in the global carbon cycle by assembling multiple diverse ecosystems and linking the terrestrial, oceanic, and atmospheric carbon reservoirs. These regions are characterized by primary production, carbon fixation, and remineralization ratios significantly higher than in the open oceans due to higher supplies of organic and inorganic carbon (Walsh, 1991; Mackenzie et al., 1998; Borges et al., 2005; Muller-Karger et al., 2005) and show a high spatio-temporal variability

in terms of air-sea CO_2 exchange, often acting as a CO_2 sink and source during cold and warm months, respectively (e.g., Frankignoulle and Borges, 2001; Cai et al., 2006; Shadwick et al., 2010, 2011). However, the air-sea CO_2 fluxes have been difficult to quantify in these areas due to the lack of underway field data and the subsequent limited number of local and regional studies. Hence, continuous high-frequency monitoring is required to assess the ocean CO_2 uptake with a higher certainty. It is important to remark and understand the role of regional areas in the climate change. In fact, the recent IPCC report 2021 (IPCC, 2021) together with the 2007 report (IPCC, 2007), highlighted the need of study of marginal seas, continental shelves, and semi-enclosed seas due to the variability on the biogeochemical cycles as well as the human pressure.

In this context, the Strait of Gibraltar (**Figure 1**) is a key region in physical and biogeochemical terms influenced by several different processes and therefore characterized by its high variability. The physical processes that govern the hydrodynamics in the Strait of Gibraltar (e.g., Lacombe and Richez, 1982; Gascard and Richez, 1985; Armi and Farmer, 1988; Bryden and Kinder, 1991) are involved in the variation of biogeochemical properties and have been analyzed in terms of physical–biological coupling in previous studies (Echevarría et al., 2002; Macias et al., 2006; Macías et al., 2007; Ramírez-Romero et al., 2014). However, the knowledge about the surface CO_2 system and air-sea fluxes is scarce due to insufficient data.

Previous studies have explored the distribution of the CO_2 system parameters in the water column (Dafner et al., 2001; Santana-Casiano et al., 2002), reported an increase in total inorganic carbon from surface to the bottom of 2068–2150 and 2307–2325 $\mu mol\ kg^{-1}$ in surface Atlantic and Mediterranean waters, respectively. The annual cycle and spatial distribution of the surface CO_2 system variables was analyzed by de la Paz et al. (2009), which accounted a seasonal change in CO_2 fugacity of $\sim$60 μatm mainly controlled by temperature fluctuations. The Atlantic–Mediterranean interaction was also assessed in terms of natural and anthropogenic carbon exchange (Huertas et al., 2009) and decadal acidification (Flecha et al., 2019). The air-sea CO_2 exchange evaluations have determined that the Strait of Gibraltar behaves as a net atmospheric CO_2 sink on an annual scale (Santana-Casiano et al., 2002; de la Paz et al., 2009, 2011). Nevertheless, these studies are based on temporarily limited observations at certain locations along the channel and new strategies for continuous monitoring of oceanic CO_2 are required to develop high spatio-temporal resolution studies of the CO_2 system in highly variables areas such as the Strait of Gibraltar.

The aim of this study was to analyze the spatio-temporal variability of the surface CO_2 system and air-sea exchange along the Strait of Gibraltar. The processes that control the distribution of the CO_2 system parameters and fluxes were attended. The latitudinal variability related to the influence of different biogeochemical processes near both the Iberian and African coasts, the interaction between the Northeast Atlantic and the Mediterranean Sea, the effect of west-to-east surface circulation and other physical processes acting on the Strait were analyzed through the northernmost and southernmost part of the channel. These data will improve our knowledge about the role of coastal regions, marginal and semi-enclosed seas and coastal to open-ocean transitional areas in terms of air-sea CO_2 exchange.

STUDY AREA

The Strait of Gibraltar (**Figure 1**) is a narrow ($\sim$20 km) and shallow ($\sim$600 m) channel with a west-to-east orientation that connects the Mediterranean Sea with the Northeast Atlantic. The minimum width at the Tarifa Narrow (TN, $\sim$14 km) and minimum depth at the Camarinal Sill (CS, $\sim$290 m) and at the Espartel Sill (ES, $\sim$360 m) play an important role in the exchange of water through the channel (e.g., Sánchez-Garrido et al., 2008, 2011; García-Lafuente et al., 2011; Sammartino et al., 2015).

The circulation pattern in the Strait has been described as a two-layer system: a surface Atlantic water inflow toward the east and a deep Mediterranean water outflow toward the west (e.g., Lacombe and Richez, 1982; Gascard and Richez, 1985; Armi and Farmer, 1988; Bryden and Kinder, 1991). The fresher and nutrient-depleted Atlantic water is separated from the saltier and nutrient-rich Mediterranean water by the Atlantic–Mediterranean Interface (AMI) layer (Lacombe and Richez, 1982; Bray et al., 1995). The AMI is deeper, thicker and colder in the westernmost part of the channel and slopes up toward the northeast from $\sim$200 m depth in ES to $\sim$75 m depth eastward of Gibraltar Central (GC) (Bray et al., 1995; Huertas et al., 2009). The shallow position of the AMI promotes the deep-water upwelling in the eastern and north-eastern region of the Strait (Minas et al., 1991; Echevarría et al., 2002; Gómez-Jakobsen et al., 2019).

The main physical components of the circulation and flow through the channel were detailed by Candela et al. (1990): a barotropic tidal flow, a barotropic sub-inertial component driven by atmospheric pressure fluctuations in the Mediterranean Sea, a long-term baroclinic component term driven by differences in density between Mediterranean Sea and Northeast Atlantic and short-period currents associated with large-amplitude internal waves. The formation of internal waves mainly occurs in the shallower area around CS and is induced by the interaction of the tidal flow with the change in bathymetry and vertical stratification through the channel (e.g., Armi and Farmer, 1988; La Violette and Arnone, 1988; Richez, 1994; Bruno et al., 2002; Alonso del Rosario et al., 2003; Vázquez-Escobar et al., 2008). Meteorological sub-inertial forcing also influences the release of these internal waves (Candela et al., 1989; Pistek and La Violette, 1999). They are propagated toward the Mediterranean on a diurnal time scale controlled by the tides and at highly variable speeds (Watson and Robinson, 1990; Richez, 1994; Sánchez-Garrido et al., 2008), while being trapped on the lee side of CS (Bruno et al., 2002). The internal waves are an important contributor to the mixing between the Mediterranean and Atlantic layers by intermittently injecting deep and nutrient-rich water into the upper layers (Wesson and Gregg, 1994; Macias et al., 2006).

The unique hydrology of the channel influenced by its circulation pattern and the generation of physical features, as well as the local climatology, are involved in the variability of the physical and biogeochemical properties in the Strait of Gibraltar.

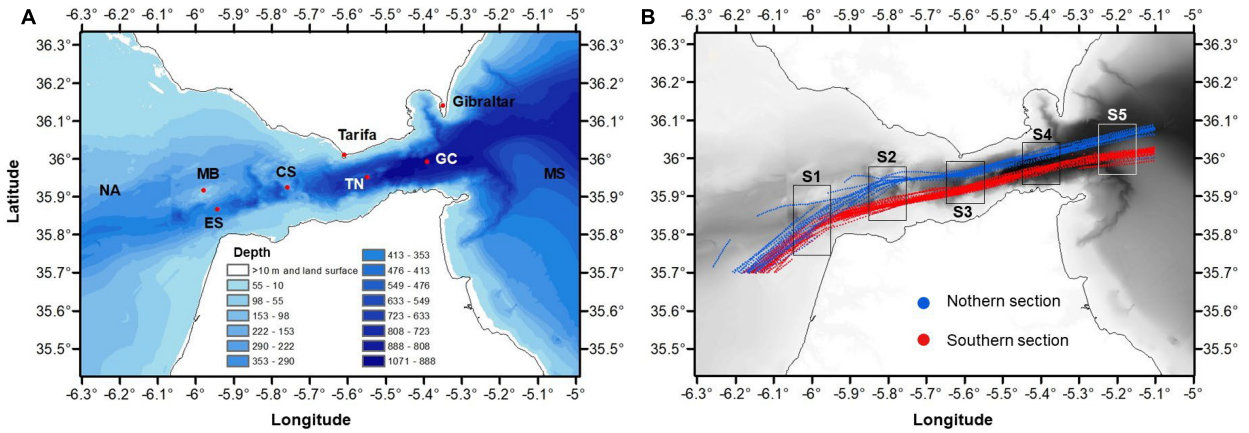

FIGURE 1 | (A) Bathymetric map of the Strait of Gibraltar and location of the topographic features of interest with west-to-east distribution: Majuan Bank (MB), Espartel Sill (ES), Camarinal Sill (CS), Tarifa Narrow (TN), and Gibraltar Central (GC). **(B)** CanOA-VOS northern (blue) and southern (red) tracks and location of the stations of interest from S1 to S5.

The tidal-induced upwelling phenomenon is combined with wind-induced upwelling events along the African coast during easterly winds (Stanichny et al., 2005) and both represent a source of high spatio-temporal variability of the surface CO_2.

MATERIALS AND METHODS

The CO_2 system and air-sea exchange was assessed in the Strait of Gibraltar based on high spatio-temporal frequency data obtained from February 2019 to March 2021 through continuous autonomous monitoring carried out by a surface ocean observation platform (SOOP) installed on a volunteer observing ship (VOS), SOOP CanOA-VOS. The SOOP CanOA-VOS was the container ship RENATE P (IMO: 9144718) operated by Nisa Marítima, which usual route runs between the Canary Islands and Barcelona, through the eastern Canary archipelago waters and northward along the northwest African and east-southeast coast of the Iberian Peninsula. Data collection and maintenance of autonomous measurement systems took place biweekly (time required to perform a round trip) at the port of Las Palmas de Gran Canaria (28.1319°N, 15.4185°W). In total, 52 routes crossed the Strait of Gibraltar: 34 upward routes through the southernmost part (southern section) and 18 downward routes through the northernmost part (northern section). The SOOP CanOA-VOS line will be part of the Spanish contribution to the Integrated Carbon Observation System (ICOS) international program in 2021. Thus, the measurement equipment and data collection process verify their quality requirements and methodological recommendations to produces comparable and high-quality dataset.

Underway Measurements and Data Collection

Autonomous monitoring was carried out by an automated underway seawater and low atmospheric CO_2 molar fraction (xCO_2) measurement system installed inside the engine room of the RENATE P container ship (Curbelo-Hernández et al., 2021). The xCO_2 measurement system, developed by Craig Neill and commercialized by General Oceanics™, combines an air and seawater equilibrator with a non-dispersive infrared analyzer for gas detection (Pierrot et al., 2009).

The system was checked automatically on departure and arrival at each port, and periodically every 3 h during the ship's journey. Four standard gasses (in the order of 0, 250, 400, and 540 ppm, with a ±0.02 ppm accuracy) provided by the National Ocean and Atmospheric Administration (NOAA) and traceable to the World Meteorological Organization (WMO) were used for system check and xCO_2 measurement corrections. Periodic calibrations were automatically performed every 12 h using standard gasses 1 and 4 to adjust the, respectively, zero and span of the infrared analyzer.

The system measures xCO_2 (ppm) in seawater with a frequency of 2–3 min and normally collect 130–150 data in the Strait of Gibraltar. The system also performs three xCO_2 measurements in low atmosphere after each calibration. In both cases, a non-dispersive infrared analyzer built by LICOR® (initially the 6262 model and after October 2019, a 7000 model) were used for the detection of xCO_2.

The sea surface temperature (SST, in °C) was measured using an SBE38 thermometer with an estimated error of 0.01°C placed at the main seawater intake. In addition, due to the high sensitivity of xCO_2 to temperature changes, an SBE45 thermosalinograph and a Hart Scientific HT1523 Handheld Thermometer, with an estimated error of ±0.01°C each, were used to monitor the temperature near the xCO_2 system and inside the equilibrator, respectively.

Sea surface salinity (SSS) was measured with a manually calibrated SBE45 thermosalinograph, with an estimated error of ±0.005. Atmospheric pressure was measured by the transducer on the deck (these pressure records being different in the order of millibars with the pressure near the xCO_2 system, inside the ship).

Due to technical problems with the measurement equipment aboard the SOOP CanOA-VOS, no measurements were obtained

during March 2019 (problems with water intake), during the second half of August 2019 and March–April 2020 (problems with LICOR flow that could not be resolved due to COVID-19 limitations) and on a limited number of return journeys from the port of Barcelona.

Determination of Variables

This study followed the data collection methodology, quality control, and calculation procedures as published in the updated version of the DOE method manual for ocean CO_2 analysis (Dickson et al., 2007). The fugacity of CO_2 was calculated in seawater ($fCO_{2,sw}$) and in the lower atmosphere ($fCO_{2,atm}$) from measured and corrected xCO_2 values following Pierrot et al. (2009).

The thermal and non-thermal contribution on $fCO_{2,sw}$ and variations was studied using the equations presented by Takahashi et al. (2002), with the temperature effects on $fCO_{2,sw}$ for isochemical seawater of $0.0423°C^{-1}$ determined experimentally by Takahashi et al. (1993). The non-thermal effect ($fCO_{2,non-thermal}$) was obtained from the seasonal amplitude of the normalized $fCO_{2,sw}$ to the average temperature (Eqs 1, 2). The thermal effect ($fCO_{2,thermal}$) was calculated by applying the observed temperature effect to the average value of $fCO_{2,sw}$ (Eq. 3) and determining its seasonal amplitude (Eq. 4). The relative importance of thermal and non-thermal effects was expressed by the T/B ratio ($\Delta fCO_{2,thermal}/\Delta fCO_{2,non-thermal}$), with values greater than 1 indicating that the temperature effect dominated over non-physics effects.

$$fCO_2\,(T_{mean}) = \left(fCO_2\right)_{obs} \cdot \exp[0.0423\,(T_{mean} - T_{obs})] \quad (1)$$

$$\left(\Delta fCO_2\right)_{bio} = [fCO_2\,(T_{mean})]_{max} - [fCO_2\,(T_{mean})]_{min} \quad (2)$$

$$fCO_2\,(T_{obs}) = \left(fCO_2\right)_{mean} \cdot \exp[0.0423\,(T_{obs} - T_{mean})] \quad (3)$$

$$\left(\Delta fCO_2\right)_{temp} = [fCO_2\,(T_{obs})]_{max} - [fCO_2\,(T_{obs})]_{min} \quad (4)$$

The CO_2 fluxes (FCO_2) were determined using Eq. 5 (Broecker and Peng, 1982) with a conversion factor of 0.24 mmol m^{-2} d^{-1}. The solubility (S, mol L^{-1} atm^{-1}) and the difference between seawater and low atmosphere fCO_2 ($\Delta fCO_2 = fCO_{2,sw} - fCO_{2,atm}$) were considered. Negative fluxes indicate that the ocean acts as an atmospheric CO_2 sink, while the positive ones indicate that it behaves as a source.

$$FCO_2 = 0.24 \cdot S \cdot k \cdot \Delta fCO_2 \quad (5)$$

The updated Wanninkhof (2014) parameterization was used in this study due to it considers the most recently advances in the quantification of the input parameters and improves the wind speed products, with k being the gas transfer rate expressed in Eq. 6:

$$k = 0.251 \cdot w^2 \cdot \left(\frac{Sc}{660}\right)^{-0.5} \quad (6)$$

where w is the wind speed (m s^{-1}) and Sc is Schmidt number (cinematic viscosity of seawater, divided by the gas diffusion coefficient). Daily averages of satellite ocean surface wind speed derived from the Advanced Scatterometer (ASCAT) and obtained from the Satellite Research and Exploitation Center (CERSAT) at IFREMER (Plouzane, France) were considered together with daily measured wind speed averages provided by the Agencia Estatal de Meteorología (AEMET) from the meteorological station located at Tarifa (Cádiz) and corrected to 10 m height (Allen et al., 1998). These wind speed data were interpolated based on the latitude, longitude, and time of the underway xCO_2 measurements. The average ocean surface wind speed for the entire study period calculated from satellite and measured data was 7.77 ± 2.66 and 8.18 ± 2.61 m s^{-1}, respectively. Due to these wind speed values were consistent, the FCO_2 was calculated in this study by considering the wind speed data measured at the Tarifa meteorological station as was done previously by de la Paz et al. (2011) to assess the air-sea CO_2 exchange in the Strait of Gibraltar.

Autonomous monitoring was combined with 25 discrete surface seawater samples taken manually from the intake seawater line for total alkalinity (A_T, μmol kg^{-1}) and total dissolved inorganic carbon (C_T, μmol kg^{-1}) in February 2020 and March 2021 with *in situ* measurements of SST and SSS. Samples were taken with a temporal frequency of 1–2 h in borosilicate glass bottles, overfilled, preserved with 100 μl of saturated $HgCl_2$, kept in darkness and analyzed just after arriving at port, in a period less than 2 weeks. The A_T was determined by potentiometrically titration in a VINDTA 3C system following Mintrop et al. (2000) and using CRMs (provided by A. Dickson at Scripps Institution of Oceanography) to test the performance of the titration system and correct the determined values. The CRMs titration gave values with and accuracy of ±1.5 μmol kg^{-1}.

The determined A_T values were consistent with those estimated according to the global relationship of A_T with SSS and SST in global surface waters described by Lee et al. (2006) for the North Atlantic (presented an average difference of 3.08 ± 6.80 μmol kg^{-1}). Due to the similarity of both values, A_T was calculated for the time, longitude, and latitude of the CanOA-VOS data using the A_T-SSS relationship obtained from the discrete samples (Eq. 7; r^2 = 0.87 and Pearson correlation coefficient given hereinafter as ρ is equal to 0.93) (temperature was not found to improve the fitting of the experimental data). It was assumed that the change in A_T with SSS was constant throughout the year in tropical and subtropical latitudes (Lee et al., 2006).

$$A_T = 2501 - 241.9 \cdot (SSS - 35) - 112.2 \cdot (SSS - 35)^2 \quad (7)$$

The C_T and pH in total scale (pH_T) were computed with the Excel program CO_2sys, using the carbonic acid dissociation constants of Lueker et al. (2000), the HSO_4 dissociation constant of Dickson (1990) and the value of $[B]_I$ determined by Lee et al. (2010). The longitudinal change in the seasonality of the variables measured *in situ* (SST and SSS), determined ($fCO_{2,sw}$ and FCO_2) and computed (C_T and pH_T) was studied in the entire region along the northern and southern sections. The C_T was normalized

(NC_T) to a constant SSS of 36.4 (the annual average SSS) to remove the effect of evaporation and precipitation. Similarly, the pH_T values were normalized ($pH_{T,18}$) to a constant SST of 18.0°C (annual average SST) to remove the temperature dependence on the variation of pH_T (Santana-Casiano et al., 2001; González-Dávila et al., 2003).

The temporal variation of C_T was studied using the equation provided by Sarmiento and Gruber (2006) (Eq. 8). This equation describes the change in C_T over time produced by air-sea CO_2 exchange (EX), horizontal advection (TRSP), vertical mixing (MIX), and net community production (NCP).

$$\frac{dNC_T}{dt} = \frac{dNC_T}{dt}|_{EX} + \frac{dNC_T}{dt}|_{TRSP} + \frac{dNC_T}{dt}|_{MIX} + \frac{dNC_T}{dt}|_{NCP} \quad (8)$$

The increase and depletion of NC_T in surface waters was studied during a whole year (February–January) using monthly average NC_T values between February 2019 and February 2021 and considering the variation of the mixed layer depth (MLD). The temporal change in NC_T was calculated as the difference between two consecutive months and was expressed in mmol m^{-3}, considering the seawater density. Negative values indicate that NC_T decreases in surface waters. The relative contribution of CO_2 exchange in the variation of NC_T (EX term) is given by the relationship between FCO_2 and MLD. The monthly MLD values were obtained with a spatial resolution of 0.028° × 0.028° from the operational Iberian–Biscay–Irish (IBI) Ocean Analysis and Forecasting system based on a (eddy-resolving) NEMO model application and are available at E.U. Copernicus Marine Service Information.[1] The annual MLD cycle was calculated using the harmonic fitting equation and parameters shown in **Supplementary Table 1**.

The relative contribution of horizontal transport (TRSP term) was calculated by considering a surface transport from the Northeast Atlantic to the Mediterranean Sea. The spatial change in NC_T between westernmost and easternmost waters [$\Delta NC_T = NC_{T,(West)} - NC_{T,(East)}$] was considered. Data available at the Surface Ocean CO_2 Atlas (SOCAT v2020[2]) referenced to 2019 have been used for the calculation of NC_T at a reference station to the west of the Strait of Gibraltar (6.75 ± 0.25°W) in a similar latitudinal range. The spatial change in salinity was removed by calculating the NC_T at all the selected locations in the Strait of Gibraltar at the constant salinity of the reference station. The horizontal transport contribution to NC_T fluctuations was obtained from the product of ΔNC_T and the change in salinity with time at the locations of interest in the Strait of Gibraltar. Positive values indicate that horizontal transport occurred in a west-to-east direction, while negative values indicated that the transport direction was reversed.

The relative contribution of vertical mixing (MIX term) was estimated following Bégovic and Copin-Montégut (2002) by considering the sum of changes in vertical diffusion across the bottom of the mixed layer and vertical entrainment into the surface layer (Eq. 9). This term was determined using the monthly values of total dissolved inorganic carbon in the MLD obtained from IBI MFC high-resolution biogeochemical forecasts and generated from the PISCES biogeochemical model and the NEMO ocean circulation model. Additional monthly values of temperature and salinity obtained from the operational IBI Ocean Analysis and Forecasting system based on a NEMO model were used to estimate the seawater density. These forecast data have a spatial resolution of 0.028° × 0.028° and are available in E.U. Copernicus Marine Service Information.[1]

$$\triangle NC_T|_{MIX} = \frac{1}{MLD} K_Z \frac{\partial NC_T}{\partial z} + \frac{1}{h}\theta\left(\frac{\partial MLD}{\partial t}\right)(NC_{T,f} - NC_T) \quad (9)$$

The difference between NC_T concentration below ($NC_{T,f}$) and at the base (NC_T) of the mixed layer was considered to calculate the term of the vertical entrainment. The function θ is equal to 0 when the mixed layer decreases ($\partial MLD/\partial t$) $\leq$ 0 due to the fact that only the deepening of the mixed layer induces mixing with the underlying waters (Peng et al., 1987; Fasham et al., 1990; Gruber et al., 1998). The vertical gradient of NC_T at the base of the mixed layer ($\partial NC_T/\partial z$) was considered for the calculation of vertical diffusion. The vertical diffusion coefficient (K_z, m^{-2} d^{-1}) at the base of the mixed layer was determined according to Denman and Gargett (1983) using Eq. 10:

$$K_z = \frac{0.25\ \varepsilon\ \rho}{g\left(\frac{\partial \rho}{\partial z}\right)} \quad (10)$$

where ρ is the seawater density at the base of the mixed layer, g is the acceleration of gravity and ε is the rate of turbulent energy dissipation. In this study we considered the vertical density gradient ($\partial\rho/\partial z$) in the pycnocline and a representative value of 2.0×10^{-8} m^2 s^{-3} for ε (Gruber et al., 1998).

Lastly, the change in NC_T due to net community production processes (NCP term), considering total changes in photosynthesis/respiration processes, was obtained directly from Eq. 8. Positive contributions of NCP indicated that the remineralization processes increase the NC_T in surface waters while negative contributions shows that biological production decrease it surface concentration.

Computational Methods

The raw output data was initially filtered removing data affected by the automatic sampler such as samples measured at low water rates (<2.5 L min^{-1}). The measured xCO_2 values were corrected following Pierrot et al. (2009) by linearly interpolating the certified standard values (section 3.2) with the xCO_2 measurement times. The three $fCO_{2,atm}$ values obtained after each calibration were averaged and harmonically interpolated with the times of each $fCO_{2,sw}$. The ΔfCO_2 was computed from the difference between the $fCO_{2,sw}$ and the $fCO_{2,atm}$ values and was used in the FCO_2 calculations (section 2.2). Additional daily average satellite data for Chlorophyll *a* obtained from the Operational Mercator Ocean biogeochemical global ocean analysis and forecast system (United States Copernicus Marine Service Information) were used to improve the understanding of the biological influence on the CO_2 system variability.

[1] https://marine.copernicus.eu/

[2] https://www.socat.info/

Chlorophyll *a* data was interpolated with latitude, longitude, and time of the CanOA-VOS line data.

The average physical and biogeochemical variables (y) for each selected station were fitted to a harmonic Eq. 11 as a function of time (x) in order to study the seasonal variability and the thermal and non-thermal effect on $fCO_{2,sw}$ (Takahashi et al., 2002; Lüger et al., 2004). The *a*–*e* coefficients are shown in **Supplementary Table 2**.

$$y = a + b\cdot\cos(2\pi x) + c\cdot\sin(2\pi x) + d\cdot\cos(4\pi x) + e\cdot\sin(4\pi x) \quad (11)$$

The results were compared to surface data collected by other VOS and research vessels in the oceanographic environment of the Strait of Gibraltar and are available at the SOCAT v2020 database. The SOCAT data between 1999 and 2019 were used to study the monthly frequency and the annual cycle of $fCO_{2,sw}$ in 2019 by considering an interannual rate of increase of 1.8 μatm per elapsed year (Bates et al., 2014).

RESULTS

The present study provides a high-resolution evaluation of the spatio-temporal variability of surface CO_2 in the Strait of Gibraltar. The annual and seasonal averages of the carbon variables in both the northern and the southern routes are presented in **Table 1** with maximum values of SST, $fCO_{2,sw}$, and FCO_2 and minimum values of C_T and pH_T during summer. The greatest seasonal change occurs from winter to summer: the SST, $fCO_{2,sw}$, and FCO_2 increased in the northern section by 4.79 ± 1.97°C, 40.75 ± 28.83 μatm, and 5.52 ± 4.19 mmol m^{-2} d^{-1}, respectively, leading to a pH_T decrease of 0.039 ± 0.028 U. The seasonal change along the southern section was slightly lower on average except for FCO_2, C_T, and NC_T (5.67 ± 5.84 mmol m^{-2} d^{-1}, 24.72 ± 19.1 μmol m^{-3}, and 23.20 ± 18.15 μmol m^{-3}, respectively). The seasonal change in pH along the southern section was 0.026 ± 0.014 U. In contrast, spring and autumn averages were similar for all the considered variables in both sections.

Spatial Distribution of Sea Surface Temperature, Sea Surface Salinity, and CO_2 System Parameters and Fluxes

The longitudinal west-to-east distribution of the variables of interest was studied (**Supplementary Figures 1**, **2**) and showed differences, especially during summer. The longitudinal variation was analyzed separately in the northern and southern sections: the SST, SSS, and CO_2 system variables and fluxes were annually and seasonally averaged every 0.05° longitude (**Figure 2**) by considering the following periods: January–March (winter), April–June (spring), July–September (summer), and October–December (autumn). The average values show that SST drives the $fCO_{2,sw}$ and FCO_2 variations. The greatest latitudinal differences were found toward the east of GC. The average SST, $fCO_{2,sw}$, FCO_2, and pH_T values follow an opposite west-to-east trend between the northern and southern sections. The

TABLE 1 | Annual and seasonal average of SST, SSS, and CO_2 system variables and fluxes with their respective standard deviations along the northern and southern sections of the Strait of Gibraltar.

Season	Section	SST (°C)		SSS		$fCO_{2,sw}$ (μ atm)		FCO_2 (mmol m^{-2} d^{-1})		C_T (μ mol kg^{-1})		NC_T (μ mol kg^{-1})		pH_T		$pH_{T,18}$	
		Mean	Standard deviation	Mean	Standard deviation	Mean	Standard deviation	Mean	Standard deviation	Mean	Standard deviation	Mean	Standard deviation	Mean	Standard deviation	Mean	Standard deviation
Winter	N	16.28	0.55	36.430	0.169	368.55	5.90	−3.76	1.49	2116.62	11.72	2115.79	9.27	8.085	0.006	8.062	0.007
	S	16.25	0.45	36.413	0.111	379.37	10.01	−4.93	3.44	2123.67	11.76	2122.91	9.72	8.074	0.010	8.047	0.015
Spring	N	18.26	1.63	36.326	0.129	379.50	19.57	−2.67	2.23	2102.85	16.13	2107.11	10.24	8.073	0.018	8.077	0.018
	S	18.08	1.61	36.298	0.130	388.65	13.84	−2.55	2.44	2108.25	13.21	2114.19	11.31	8.064	0.013	8.065	0.021
Summer	N	21.07	1.61	36.371	0.194	409.30	24.26	1.76	3.30	2098.39	8.97	2100.08	8.10	8.046	0.023	8.093	0.015
	S	20.82	2.30	36.387	0.162	406.34	21.40	0.74	3.71	2098.95	11.65	2099.72	12.35	8.048	0.019	8.091	0.022
Autumn	N	18.71	1.17	36.432	0.189	385.84	13.39	−2.92	2.65	2111.26	15.89	2109.43	10.61	8.068	0.014	8.076	0.017
	S	18.70	1.67	36.501	0.132	384.33	9.27	−3.13	2.59	2111.75	14.22	2105.94	14.28	8.070	0.009	8.080	0.027
Annual	N	18.02	2.14	36.398	0.175	383.10	22.35	−2.14	3.19	2108.47	15.12	2109.21	11.23	8.071	0.021	8.075	0.018
	S	17.86	2.11	36.415	0.144	385.90	15.26	−3.10	3.68	2114.40	15.41	2113.55	14.72	8.068	0.014	8.066	0.027

seasonality of SST and $fCO_{2,sw}$ was maximum (5.29 ± 2.97°C and 45.51 ± 28.11 μatm, respectively) in the westernmost part (6.15–5.95°W) and minimum in the eastern area closest to the Mediterranean Sea (5.30–5.10°W) in both the northern (4.47 ± 2.68°C and 19.11 ± 24.86 μatm, respectively) and the southern (3.39 ± 2.11°C and 23.81 ± 14.96 μatm, respectively) sections. The seasonal change in pH_T (northern and southern sections, respectively) was 0.053 ± 0.028 and 0.033 ± 0.024 U in the westernmost part and 0.019 ± 0.025 and 0.025 ± 0.015 U in the easternmost part.

An annual average west-to-east decrease through the northern and southern routes was obtained for SST [1.70°C (r^2 = 0.64 and ρ = −0.80) and 1.48°C (r^2 = 0.83 and ρ = −0.91) per degree of longitude, respectively] and $fCO_{2,sw}$ [14.21 μatm (r^2 = 0.65 and ρ = −0.81) and 2.71 μatm (r^2 = 0.22 and ρ = −0.47) per degree of longitude, respectively] (**Figures 2A,E**). The seasonality of pH_T increased toward the east in both sections (**Figure 2G**) and correlated with the decrease in $fCO_{2,sw}$ (−0.001 U μatm^{-1}, $r^2 > 0.94$, and $\rho < -0.97$). These longitudinal changes were maximum during summer in the northern section: SST and $fCO_{2,sw}$ decreased by 2.95°C (r^2 = 0.66 and ρ = −0.81) and 47.47 μatm (r^2 = 0.87 and ρ = −0.93) per degree of longitude, respectively, while the pH_T increased by 0.047 U (r^2 = 0.86 and ρ = 0.93) per degree of longitude.

The annual average FCO_2 (**Figure 2E**) shows that the CO_2 sink increased toward the east in both the northern (−1.89 mmol m^{-2} d^{-1} per degree of longitude, r^2 = 0.68, and ρ = 0.82) and the southern (−1.27 mmol m^{-2} d^{-1} per degree of longitude, r^2 = 0.57, and ρ = 0.75) sections. The west-to-east increasing sink gradient was most intense during spring [−2.23 (r^2 = 0.34 and ρ = 0.58) and −1.38 (r^2 = 0.64 and ρ = 0.80) mmol m^{-2} d^{-1} per degree of longitude, respectively] and summer [−6.71 (r^2 = 0.89 and ρ = 0.94) and −2.69 (r^2 = 0.60 and ρ = 0.77) mmol m^{-2} d^{-1} per degree of longitude, respectively]. During summer, both the northern and southern sections behaved as a CO_2 source (3.11 ± 1.76 and 1.24 ± 3.84 mmol m^{-2} d^{-1}, respectively) in the westernmost part (6.15–5.5°W) and as a weak CO_2 sink (−0.87 ± 2.62 and −0.57 ± 2.48 mmol m^{-2} d^{-1}) in the easternmost part (5.5–5.1°W). Maximum outgassing was found in both the northern and southern sections during summer around ES (4.49 ± 2.45 and 2.28 ± 3.91 mmol m^{-2} d^{-1}, respectively) and TN (2.99 ± 0.74 and 2.20 ± 2.59 mmol m^{-2} d^{-1}, respectively). In contrast, maximum ingassing was obtained along the northern section between ES and CS during autumn (−6.01 ± 0.05 mmol m^{-2} d^{-1}) and toward the east of TN along the southern section during winter (−6.57 ± 4.11 mmol m^{-2} d^{-1}).

The longitudinal change in SSS (**Figure 2B**) was significant in this transition area between Northeast Atlantic and Mediterranean Sea waters and influenced the spatial distribution of C_T. Big differences in SSS and C_T values were observed between the northern and southern sections. In the northern section, the annual average of SSS slightly decreased from the most Atlantic part to GC (0.12 U per longitude, r^2 = 0.66, and ρ = −0.81) and increased rapidly toward the east of GC (1.40 U per longitude, r^2 = 0.95, and ρ = 0.97). These longitudinal changes were also observed in the southern section, but both the decrease (0.08 U per degree of longitude, r^2 = 0.67, and ρ = −0.82) and the increase (0.50 U per degree of longitude, r^2 = 0.86, and ρ = 0.93) were lower.

The longitudinal distribution of C_T (**Figure 2D**) was correlated with that of SSS in the northern section (r^2 = 0.91 and ρ = 0.95), while this control was not observed in the southern section (r^2 = 0.13 and ρ = 0.36). The average annual NC_T (**Figure 2F**) increased similarly toward the east in both the northern (11.42 μmol kg^{-1} per degree of longitude, r^2 = 0.64, and ρ = 0.80) and the southern sections (12.64 μmol kg^{-1} per degree of longitude, r^2 = 0.80, and ρ = 0.89). The average NC_T values were maximum during the cold months (January–June) and minimum during the warm months (July–December) in the entire region, except in the northern section during autumn to the east of CS and during summer around TN. The decrease in $fCO_{2,sw}$ between CS and GC in summer and the effects of remineralization and vertical mixing processes accounted for these changes. The absolute minimum values of NC_T in summer along each route should be highlighted: the minimum value eastward of GC in the northern section (2090.60 ± 4.99 μmol kg^{-1}) was followed by a reduction of the oceanic CO_2 sink and high values of $fCO_{2,sw}$, while that of the southern route in TN (2090.03 ± 2.95 μmol kg^{-1}) coincided with maximum values of SST, $fCO_{2,sw}$, and FCO_2 and may be related to an increase in biological production.

Seasonality of the CO_2 System and Fluxes

The seasonality of SST, SSS, and CO_2 system variables and fluxes were studied on both the northern and the southern routes (**Supplementary Figures 3**, **4**) by averaging the values obtained on each trip and fitting them to a harmonic Eq. 11. The average values of $fCO_{2,sw}$ and pH ranged between ∼360 and 430 μatm and between ∼8.03 and 8.09, respectively, in phase with a seasonal temperature change of ∼7.5°C (between ∼15.5 and 23.0°C). Several differences were observed between the northern and the southern sections: the $fCO_{2,sw}$ and pH trends (**Supplementary Figure 3**) show a lower seasonality along the southern route despite the fact that the seasonal change in SST is maximum in this section. The $fCO_{2,sw}$ values were compared with surface $fCO_{2,sw}$ data available at the SOCAT v2020 database for the Strait of Gibraltar between 1999 and 2019 (**Supplementary Figure 5**). The CanOA-VOS lines provided a total of 6440 measurements during the 2 years of study (2019–2021), almost the same number of observations (6063 data) as in the SOCAT database for a period of 20 years (1999–2019). The CanOA-VOS line collected data at times of the year when there was no previous data available (February, May–July, and December). The annual cycle of $fCO_{2,sw}$ provided from both the CanOA-VOS and the SOCAT databases is described by Eqs 12, 13 (r^2 = 0.67 and r^2 = 0.64, respectively) in which SST fluctuations were considered (SSS was not found to improve the fitting). Their standard errors of estimate was ±10.2 and ±13.8 μatm, respectively.

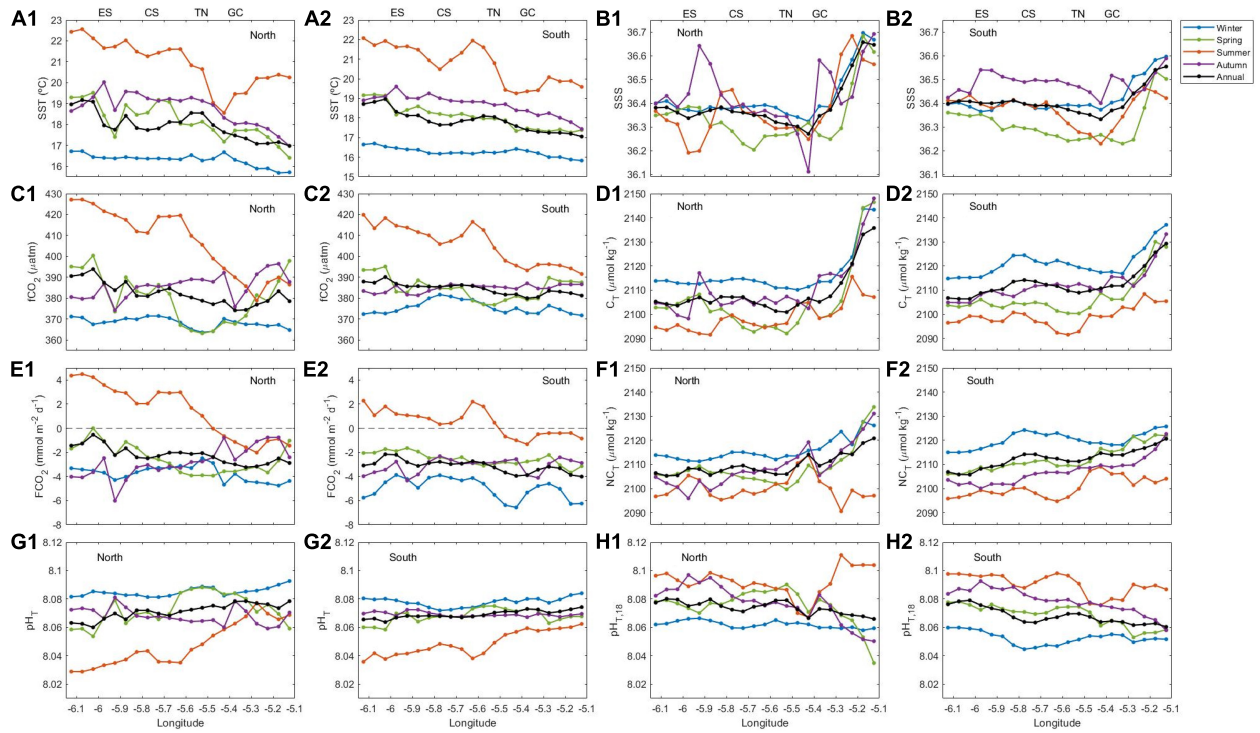

FIGURE 2 | Annual and seasonal average of **(A)** SST, **(B)** SSS, **(C)** $fCO_{2,sw}$, **(D)** C_T, **(E)** FCO_2, **(F)** NC_T, **(G)** pH_T, and **(H)** $pH_{T,18}$ every 0.05° of longitude along the (1) northern and (2) southern sections in the Strait of Gibraltar.

$$fCO_{2,sw}^{CanOA-VOS} = 1118.00 + 0.16^{*}\cos\left(0.53^{*}Month\right) - 15.14^{*}$$
$$\sin\left(0.53^{*}Month\right) + 2.10^{*}SST^{2} - 78.81^{*}SST \quad (12)$$

$$fCO_{2,sw}^{SOCAT} = 760.60 + 2.29^{*}\cos\left(0.55^{*}Month\right) - 12.74^{*}$$
$$\sin\left(0.55^{*}Month\right) + 1.18^{*}SST^{2} - 42.54^{*}SST \quad (13)$$

The seasonal change of $fCO_{2,sw}$ with SST obtained through the northern and southern sections of the CanOA-VOS line is given by Eqs 14, 15 (r^2 = 0.78 and r^2 = 0.66, respectively) with a standard error of estimate of ±10.3 and ±8.9 μatm, respectively.

$$fCO_{2,sw}^{CanOA-VOS-North} = 914.40 + 4.38^{*}\cos\left(0.54^{*}Month\right)$$
$$-11.36^{*}\sin\left(0.54^{*}Month\right) + 1.73^{*}SST^{2} - 60.88^{*}SST \quad (14)$$

$$fCO_{2,sw}^{CanOA-VOS-South} = 1118.00 - 2.00^{*}\cos\left(0.53^{*}Month\right)$$
$$-14.84^{*}\sin\left(0.53^{*}Month\right) + 2.08^{*}SST^{2} - 78.82^{*}SST \quad (15)$$

When the full data set (SOCAT and CanOA) was considered (more than 12,000 data), Eq. 16 (r^2 = 0.62), which present a standard error of estimate of ±12.8 μatm, provides an estimation of the interannual trend (2.33 ± 0.06 μatm year^{-1}), the seasonal variability and the influence of SST as the variable controlling the physical characteristics of the Strait of Gibraltar.

$$fCO_{2,sw} = 779.6 + 2.35^{*}(year - 1999) + 3.80^{*}\cos\left(0.56^{*}Month\right)$$
$$-11.70^{*}\sin(0.56^{*}Month) + 1.34^{*}SST^{2} - 48.89^{*}SST \quad (16)$$

The FCO_2 seasonal trend (**Supplementary Figure 3**) ranged between −6 and 3 mmol m^{-2} d^{-1} in the northern section and between −8 and 3 mmol m^{-2} d^{-1} in the southern section, with a strong behavior as a sink during the cold months and as a weak source during the warm months. The maximum outgassing (2.99 ± 2.70 and 3.60 ± 1.76 mmol m^{-2} d^{-1} in the northern and the southern section, respectively) occurred in August 2020 and coincided with high values of SST and $fCO_{2,sw}$, while the maximum ingassing (−11.48 ± 1.36 mmol m^{-2} d^{-1}) was observed along the southern section in February 2021 and was related with wind speed values higher than 11 m s^{-1}. The change in FCO_2 was linked to the change in ΔfCO_2, which is controlled by temperature fluctuations: the average values of FCO_2 increased by 1.22 mmol m^{-2} d^{-1} °C^{-1} (r^2 = 0.71 and ρ = 0.84) in the northern section and 1.03 mmol m^{-2} d^{-1} °C^{-1} (r^2 = 0.50 and ρ = 0.71) in the

southern section. A smoothing spline with a parameter of 0.98 was applied to the daily distribution of SSS ($r^2 > 0.27$), SST ($r^2 > 0.82$), $fCO_{2,atm}$ ($r^2 > 0.94$), $fCO_{2,sw}$ ($r^2 > 0.56$), and wind speed ($r^2 > 0.49$). Daily values of FCO_2 were calculated from these computed variables and fitted to the observed FCO_2 values to improve the evaluation of its temporal distribution. These computed FCO_2 values differ in average by -0.25 mmol m^{-2} d^{-1} in the northern section and by 0.15 mmol m^{-2} d^{-1} in the southern section compared to those calculated from the observed data.

The west-to-east differences were assessed by selecting five stations equidistantly spaced every 0.2° of longitude along the channel (6.0–5.2°W) (**Figure 3** and **Supplementary Figures 6**, **7**). The westernmost station at 6.0 ± 0.05°W (S1) is located near ES and was used to study the seasonality in the most Atlantic part over the main gateway of the Mediterranean outflow. The station at 5.8 ± 0.05°W (S2) was selected near the shallower area of CS. The stations at 5.6 ± 0.05°W (S3) and 5.4 ± 0.05°W (S4) were in the longitudinal range around TN and GC, respectively, over the deepest area of the channel. Lastly, the easternmost station at 5.2 ± 0.05°W (S5) was used to study the most Mediterranean part. To consider the observed latitudinal variation, the northern and southern parts of each station were represented separately at all stations except S1 due to upward and backward routes passing through the same latitudinal interval in the westernmost part. A lower temporal resolution was obtained along the northern part of the channel and at S5 (**Supplementary Figure 6**) due to technical problems with the measurement equipment and subsequent scarcity of data during the first year of observation. Hence, the harmonic fitting is useful to understand the temporal change during periods of lack of data, but the seasonal trend shows a higher uncertainty in these positions.

The latitudinal differences are greater in the most Mediterranean part of the channel. The seasonality of the SST (**Figure 3** and **Supplementary Figure 6**) decreased toward the east through the northern route (in the range between 16–23°C at S1 and 16–20°C at S4) and remained constant with longitude through the southern route (16–23°C). The $fCO_{2,sw}$ values (**Figure 3** and **Supplementary Figure 6**) were maximum at S1 throughout the year (ranging between 370 μatm during the cold months and 428 μatm during the warm months), and its seasonality remained constant along the southern section between 370 and 415 μatm in phase with temperature and influenced by non-thermal processes. The west-to-east pattern in $fCO_{2,sw}$ seasonality along the northern section was difficult to characterize due to the lack of values at certain times of the year. However, a slight increase in the seasonal signal was observed from the Atlantic part at S1 (∼57 μatm, between 371 and 428 μatm) to TN at S3 (61 μatm, between 357 and 418 μatm) and a drastic decrease toward the east in GC at S4 (34 μatm, between 362 and 396 μ atm).

The pH_T values (**Figure 3** and **Supplementary Figure 6**) were correlated with $fCO_{2,sw}$ ($r^2 > 0.98$ and $\rho = -0.99$) throughout the region and decreased by 0.001 U μatm^{-1} at all stations. The maximum seasonality was found at S1 (8.028–8.080) and in the northern sections of S3 (8.037–8.095). The greatest differences at S2 were observed during the cold months between January and May and could be related with mixing, biological and other non-thermal processes. In GC at S4, the pH_T showed minimum pH_T seasonality ranging from 8.056 to 8.089 in the northern section and from 8.039 to 8.081 in the southern section.

The FCO_2 values (**Figure 3** and **Supplementary Figure 6**) show a slight maximum outgassing and minimum ingassing in the northern part of each station. The outgassing weakened and the ingassing reinforced toward the east, reaching negative FCO_2 values along both the northern and the southern section during the entire first year of monitoring and in the northern part of S4 throughout the study period. A strong CO_2 sink was obtained at all stations during the cold periods, while the system behaved as a weak source during the warm months.

The influence of Mediterranean Sea waters on the distribution of SSS was only observed to the east of GC at S5 through the northern section (**Supplementary Figure 7**), where the values were maximum throughout the year (∼36.4–36.7). The west-to-east surface circulation from the Northeast Atlantic is reflected in the SSS between ES (S1) and GC (S4): the observed values and seasonality were minimum in the westernmost part at S1 (∼36.3–36.5) and slightly increased through the southern section between S2 and S4 (∼36.3–36.6).

The NC_T (**Supplementary Figure 7**) decreases between February and September and increases between October and January. The seasonality of C_T and NC_T in ES (S1) (∼30 μmol kg^{-1}, between 2090 and 2120 μmol kg^{-1}) increased through the southern section (∼40 μmol kg^{-1}, between 2090 and 2130 μmol kg^{-1}) and decreased through the northern section (∼15 μmol kg^{-1}, between 2100 and 2115 μmol kg^{-1}) in CS (S2) and TN (S3). In GC at S4, the seasonality decreased in the southern section (∼30 μmol kg^{-1}, between 2093 and 2123 μmol kg^{-1}) and increased in the northern section (∼22 μmol kg^{-1}, between 2098 and 2120 μmol kg^{-1}). Considering the temporal distribution of Chlorophyll *a* (**Supplementary Figure 7**), the seasonal change was reduced and the latitudinal differences increased toward the interior of the channel.

DISCUSSION

High-Resolution Study of the Spatio-Temporal Variability of the CO_2 System

The current study provides a high spatio-temporal resolution evaluation of the surface CO_2 distribution based on high-frequency underway measurements obtained during 2 entire years of observation (February 2019–March 2021). More than 6000 data obtained during those 2 years is the same amount of data available in the SOCAT database for the last 20 years.

According with the high-resolution measurements carried out in this investigation, the seasonal changes in the CO_2 system and fluxes in the Strait of Gibraltar were controlled by the annual cycle of the Atlantic inflow and the position of the AMI. These processes has been shown to control other variables in the region (e.g., Bryden et al., 1994; Bray et al., 1995; Gómez et al., 2000;

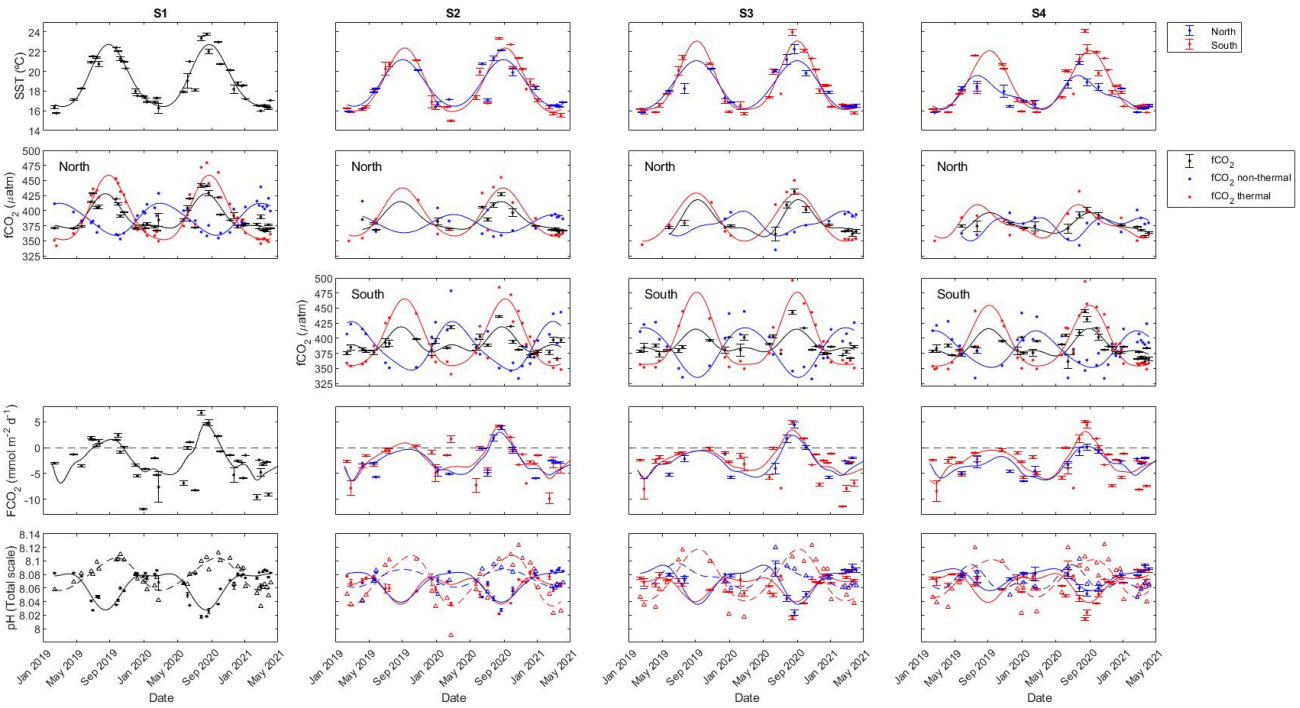

FIGURE 3 | Seasonal variability of average SST, $fCO_{2,sw}$, $fCO_{2,thermal}$, $fCO_{2,non-thermal}$, FCO_2, pH_T, and $pH_{T,18}$ at the northern (blue) and southern (red) part of the station S1–S4 in the Strait of Gibraltar.

Skliris and Beckers, 2009). The shallower depth of the AMI favors the deep, cold and CO_2-rich Mediterranean water injection into the upper layers (de la Paz et al., 2009). The AMI elevates toward the northeast throughout the year and reaches minimum depth during late winter (February–March), coinciding with an observed decrease in SST (**Figure 2A** and **Supplementary Figure 1**) and increase in SSS and Chlorophyll *a* (**Figure 2B** and **Supplementary Figure 2**). The position of the AMI is also influenced by the tidal amplitude variation and internal wave generation (Gascard and Richez, 1985; Gómez et al., 2001), which favor intermittent vertical mixing events and increase the surface CO_2 during high tides (Wesson and Gregg, 1994; Macias et al., 2006) and especially during the most energetic spring tides (García-Lafuente et al., 2000).

The spatial variability of the CO_2 system during summer is also influenced by mixing processes driven by local climatology factors, as the wind-induced upwelling in the Gulf of Cádiz, the Strait of Gibraltar and the Alboran Sea at local (e.g., Peliz et al., 2009; Gómez-Jakobsen et al., 2019; Bolado-Penagos et al., 2020) and regional scale (e.g., Richez and Kergomard, 1990; Folkard et al., 1997; Stanichny et al., 2005). The signal of the wind-induced upwelling during the warm months was observed in minimum values of SST around CS and between TN and GC (**Figure 2**). The lowest $fCO_{2,sw}$ values obtained during summer along the southern section in the westernmost part are explained by the enhancement of the biological uptake in this area due to wind-induced upwelling events at this time of the year (Stanichny et al., 2005). The opposite occurs to the east of TN, where the wind-induced upwelling weakened and higher $fCO_{2,sw}$ were encountered along the southern route during summer (**Figure 2C**). The influence of the physical variability in the seasonality of $fCO_{2,sw}$ in the area were described in term of a second degree function of SST in Eqs 12–16. The spatio-temporal variability observed in the CO_2 system and fluxes and their causes is consistent with previous studies based on datasets obtained from oceanographic surveys at certain locations and times of the year (Dafner et al., 2001; Santana-Casiano et al., 2002; de la Paz et al., 2008, 2009, 2011; Flecha et al., 2019).

The seasonality of the $fCO_{2,sw}$ values obtained in this study agreed with that obtained from SOCAT data (**Supplementary Figure 5**) and both followed SST fluctuations. A high coincidence was found in the annual cycle, with an average difference in $fCO_{2,sw}$ values between both databases of 6.94 ± 16.93 µatm. The fitting of the CanOA-VOS data and the standard error of estimate in the northern and southern section (Eqs 14, 15) and in the entire region (Eq. 12) were slightly enhanced with respect to the SOCAT data (Eq. 13) due to the higher temporal resolution in the entire annual cycle. The combination of the CanOA-VOS and SOCAT data provided an Eq. 16 that can be used to estimate $fCO_{2,sw}$ in the surface waters of the Strait of Gibraltar. The $fCO_{2,sw}$ is increasing in the Strait of Gibraltar at a rate of 2.35 ± 0.06 µatm year^{-1}, which is close to the Northeast Atlantic ESTOC site (1.92 ± 0.24 µatm year^{-1}) and similar to the Irminger Sea site (2.37 ± 0.49 µatm year^{-1}), where also vertical

mixing processes contributed to the increased observed trend (Bates et al., 2014).

Thermal and Non-thermal Control Over the CO_2 System Variability

The coupling between thermal and non-thermal processes drives the seasonal variation of the CO_2 system throughout the region. These non-thermal processes are mainly biological production (including the organic matter production and remineralization) and physical processes that are strongly coupled affecting the fCO_2 distribution with both positive and negative effects (Takahashi et al., 1993). The T/B ratios (**Table 2**) show that $fCO_{2,sw}$ seasonality in the Strait of Gibraltar was mainly controlled by thermal processes in the entire region, coinciding with previous studies in the Strait of Gibraltar (de la Paz et al., 2009) and along the northwest African coast (Curbelo-Hernández et al., 2021). However, the seasonality of $fCO_{2,thermal}$ and $fCO_{2,non-thermal}$ (**Figure 3**) and the T/B ratios obtained in the northern and the southern sections of each station show a high spatial variability in thermal and non-thermal coupling. The relevance of non-thermal processes in the temporal variation of $fCO_{2,sw}$ (**Figure 3**) was greater along the southern section due to greater influence and intensity of upwelling throughout the African coast (Stanichny et al., 2005). The non-thermal effect was maximum and close to canceling the thermal effect to the south of CS, where the tidal dynamics is enhanced and vertical mixing processes are intense (Echevarría et al., 2002). The non-thermal effect decreased from S2 to S5 through the southern section and increased from S3 to S5 through the northern section, which is related to the high-intensity upwelling in the Northwest Alboran Sea and suppression of vertical mixing to the south (Minas et al., 1991; Echevarría et al., 2002; Gómez-Jakobsen et al., 2019).

The influence of thermal processes on the temporal variation of $fCO_{2,sw}$ was also analyzed through the $fCO_{2,sw}$-SST relationship (**Table 2**). The increase in $fCO_{2,sw}$ with temperature through the northern route (9.02 ± 1.99 μatm $°C^{-1}$, $r^2 = 0.86$, and $\rho = 0.93$) doubled that obtained through the southern route (4.51 ± 1.66 μatm $°C^{-1}$, $r^2 = 0.48$, and $\rho = 0.69$). Thus, the control of thermal processes was even higher in the northern section, while in the southern section the relevance of non-thermodynamic processes increased due to the enhancement of vertical mixing and biological activity (Santana-Casiano et al., 2002). The $fCO_{2,sw}$-SST relationship is consistent with the T/B ratios obtained at each station (**Table 2**). The highest correlation and change of $fCO_{2,sw}$ with SST was obtained in the westernmost part at S1 and in the northern sections of S2 and S3 (>8.5 μatm $°C^{-1}$, $r^2 > 0.67$, and $\rho > 0.82$). In the southern sections of CS and TN, the change and correlation of $fCO_{2,sw}$-SST was found to be minimal ($r^2 < 0.28$ and $\rho < 0.53$).

The influence of non-thermal processes on the NC_T change was studied through the relationship NC_T-$fCO_{2,non-thermal}$ (**Table 2**). The NC_T increased with respect to $fCO_{2,non-thermal}$ by 0.50 ± 0.03 μmol kg^{-1} μatm^{-1} ($r^2 > 0.92$ and $\rho > 0.96$) throughout the region, but decreased with respect to $fCO_{2,thermal}$ by 0.22 ± 0.06 ($r^2 = 0.82$ and $\rho = -0.91$) and 0.34 ± 0.06 ($r^2 = 0.83$ and $\rho = -0.91$) μmol kg^{-1} μatm^{-1} through the northern and southern routes, respectively. The NC_T showed a direct relationship and correlated with $fCO_{2,non-thermal}$ (between 0.46 and 0.52 μmol kg^{-1} μatm^{-1}; $r^2 > 0.85$ and $\rho > 0.92$) at all stations. Hence, the NC_T variation was mainly driven by non-thermal processes (Santana-Casiano et al., 2002; de la Paz et al., 2008, 2009).

Seasonal Variability of NC_T and Relative Influence of Air-Sea Exchange, Biological Activity, Horizontal Transport, and Vertical Mixing

The annual cycle of C_T was studied at each of the selected stations by considering its temporal change between consecutive months. The C_T was normalized to a constant salinity of 36.4 to remove the effect of precipitation and evaporation and study the other non-conservative processes involved in the surface variation of C_T (i.e., primary production, oxidation of organic matter, precipitation/dissolution of $CaCO_3$, air-sea CO_2 fluxes, and physical processes) (e.g., Chen and Pytkowicz, 1979; Takahashi et al., 1993; Wanninkhof and Feely, 1998; Lee et al., 2000).

The results allow to establish the relative contribution of biological activity, air-sea exchange, horizontal transport, and vertical mixing (Eq. 8) on the increase and depletion of NC_T in surface waters (**Figure 4** and **Table 3**). The greatest seasonal changes of NC_T were found at S1 and throughout the southern section, especially at S2 and S3 (**Table 3**). A high spatial variability was found in the seasonality of NC_T. The depletion of NC_T

TABLE 2 | Ratios T/B and linear relationship of $fCO_{2,sw}$-SST and NC_T-$fCO_{2,non-thermal}$ at the northern and southern part of the selected stations along the Strait of Gibraltar.

Station	Section	Ratio T/B	$fCO_{2,sw}$-SST (μ atm $°C^{-1}$)	NC_T-$fCO_{2,non-thermal}$ (μ mol kg^{-1} μ atm^{-1})
S1		1.85 ± 0.12	8.50 ± 1.41 ($r^2 = 0.78$ and $\rho = 0.88$)	0.46 ± 0.04 ($r^2 = 0.93$ and $\rho = 0.96$)
S2	N	1.80 ± 0.19	8.50 ± 2.57 ($r^2 = 0.77$ and $\rho = 0.88$)	0.46 ± 0.06 ($r^2 = 0.95$ and $\rho = 0.97$)
	S	1.09 ± 0.17	2.94 ± 2.43 ($r^2 = 0.16$ and $\rho = 0.40$)	0.50 ± 0.03 ($r^2 = 0.98$ and $\rho = 0.99$)
S3	N	2.07 ± 1.86	9.04 ± 3.98 ($r^2 = 0.67$ and $\rho = 0.82$)	0.48 ± 0.12 ($r^2 = 0.87$ and $\rho = 0.93$)
	S	1.17 ± 0.11	3.78 ± 2.36 ($r^2 = 0.28$ and $\rho = 0.53$)	0.49 ± 0.03 ($r^2 = 0.98$ and $\rho = 0.99$)
S4	N	1.30 ± 0.51	5.74 ± 3.94 ($r^2 = 0.41$ and $\rho = 0.64$)	0.50 ± 0.10 ($r^2 = 0.89$ and $\rho = 0.94$)
	S	1.19 ± 0.07	5.42 ± 2.14 ($r^2 = 0.41$ and $\rho = 0.64$)	0.49 ± 0.03 ($r^2 = 0.97$ and $\rho = 0.98$)
S5	N	1.14 ± 0.68	6.01 ± 6.25 ($r^2 = 0.19$ and $\rho = 0.44$)	0.52 ± 0.10 ($r^2 = 0.89$ and $\rho = 0.94$)
	S	1.88 ± 1.35	9.03 ± 4.64 ($r^2 = 0.65$ and $\rho = 0.81$)	0.46 ± 0.14 ($r^2 = 0.85$ and $\rho = 0.92$)

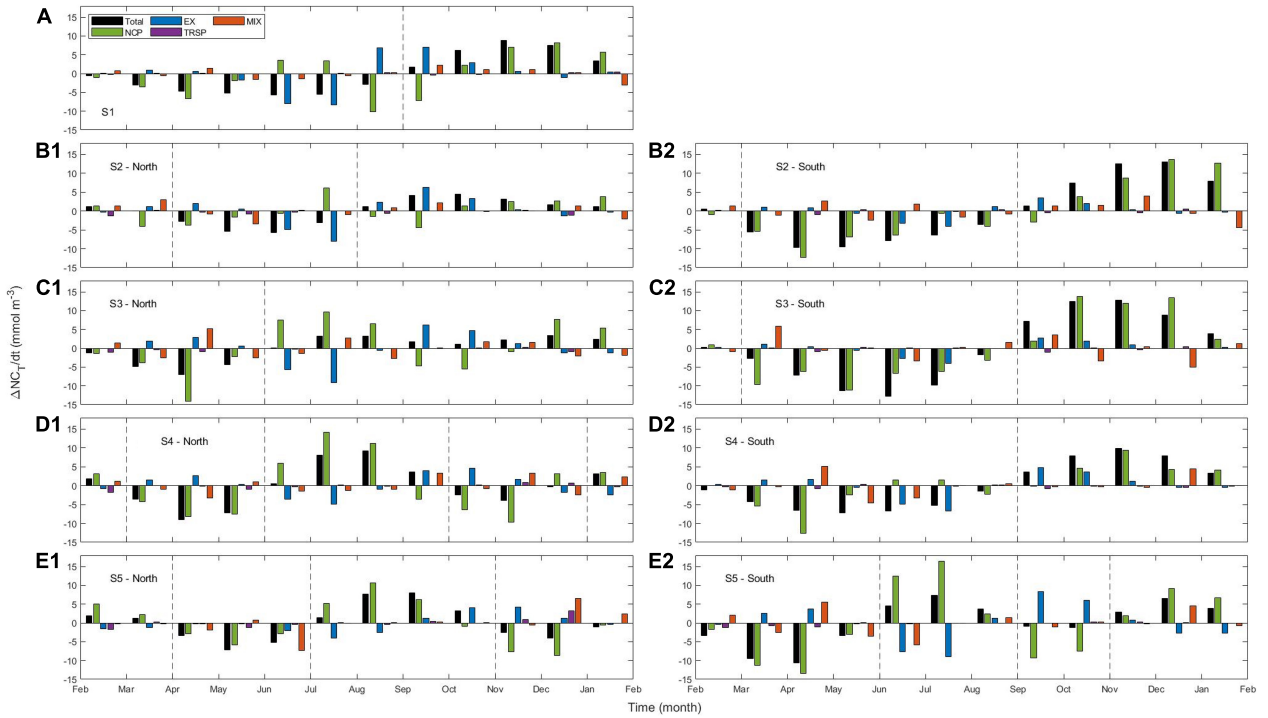

FIGURE 4 | Monthly change in NC_T ($\Delta NC_T/dt$; black) and relative contribution of net community production ($\Delta NC_T/dt|_{NCP}$; green), air-sea exchange ($\Delta NC_T/dt|_{EX}$; blue), horizontal transport ($\Delta NC_T/dt|_{TRSP}$; purple), and vertical mixing ($\Delta NC_T/dt|_{MIX}$; orange) in an entire annual cycle. The temporal variation of NC_T was evaluated in S1 **(A)** and in the northernmost and southernmost part of S2 **(B)**, S3 **(C)**, S4 **(D)**, and S5 **(E)**. The net contribution of each term in the increase and depletion of NC_T is shown in **Table 4**.

TABLE 3 | Seasonal change of NC_T ($\Delta NC_T/dt$) and net contribution of the net community production ($\Delta NC_T/dt|_{NCP}$; green), air-sea exchange ($\Delta NC_T/dt|_{EX}$; blue), horizontal transport ($\Delta NC_T/dt|_{TRSP}$; purple), and vertical mixing ($\Delta NC_T/dt|_{MIX}$; orange) in the increase and depletion of NC_T at stations S1–S5.

		S1	S2		S3		S4		S5	
			North	South	North	South	North	South	North	South
TOTAL		27.55	16.93	42.65	17.24	45.44	26.36	32.50	23.38	28.96
NCP	Increase	15.95	1.78	34.90	18.19	44.70	34.27	22.19	28.50	49.01
	Depletion	−16.43	0.07	−35.79	−21.60	−42.84	−32.79	−19.94	−28.50	−46.15
EX	Increase	9.90	11.57	5.06	0.16	5.96	−8.85	8.58	−3.90	−19.99
	Depletion	−9.64	−10.63	−5.06	5.45	−5.96	8.85	−8.37	2.87	20.03
TRSP	Increase	0.10	−2.63	−0.23	−0.76	−1.09	−2.21	−1.62	−1.22	−0.06
	Depletion	0.10	−1.36	−0.22	−2.51	−0.37	0.69	−0.43	2.25	−2.84
MIX	Increase	1.60	6.21	2.93	−0.35	−4.12	3.15	3.35	−0.01	−0.83
	Depletion	−1.57	−5.02	−1.58	1.32	3.72	−3.11	−3.77	−0.07	0.86

in the southwestern part occurred from February–March to September, while it was difficult to establish a seasonal pattern through the northern section and in the easternmost part due to the high variability of the surface inflow in the tidal time-scale (de la Paz et al., 2009).

The seasonal change of NC_T was controlled by NCP processes at most of the stations except in the northern part at S2 (0.4–10.6%; **Figure 4B**), where the air-sea exchange and vertical mixing dominated (62.7–68.4 and 29.7–36.7%, respectively) and horizontal transport influenced (8.0–15.6%). It is related to the generation of internal bores at CS (Boyce, 1975; Armi and Farmer, 1988; Bruno et al., 2002) and the minimum intensity of the wind-induced upwelling toward the northwest of the channel (Peliz et al., 2009). The biological effect was especially significant along the African coastal upwelling (Stanichny et al., 2005) in the southern part of S2 (81.8–83.9%) and S3 (94.2–98.4%). The upwelling effect in the Northwest Alboran Sea (Minas et al., 1991; Echevarría et al., 2002; Gómez-Jakobsen et al., 2019) was detected at the easternmost stations (**Figures 4D,E**). The change in NC_T explained by NCP exceeded the total change of NC_T

by 24.4–30.0 and 21.9–69.3% in the northern part at S4 and S5, respectively. The biological effect in these locations was counteracted by the contribution of air-sea exchange (12.3–33.6% in the northern part at S4 and S5 and 69.04–69.2% in the southern part at S5) and the influence of vertical mixing and horizontal transport (<12 and <10%, respectively). The contribution of NCP is strongly linked to the vertical mixing processes in this region, which inject deeper and remineralized CO_2-rich water in surface layers. Positive contributions of vertical mixing indicated that the NC_T increase in the surface layer due to the deep-water injection, while negative values indicate that the concentration of NC_T on the surface is higher than in depths layers due to a minimal biological production on the surface. In some periods, the amount of injected CO_2 to the surface is not counterbalanced by primary production and positive values contributed to the observed monthly variability. Accordingly, the seasonal and spatial variation of the AMI and the deep water injection processes in the surface layers drove by the wind (wind-induced upwelling) through the southernmost part and by tides (tidal-induced upwelling) through the northernmost part could account for the observed positive and negative contributions of both NCP and vertical mixing. The contribution of vertical mixing was especially significant in certain locations due to the advection of C_T in upper layers toward the east of CS during tidal-induced upwelling events (de la Paz et al., 2008). The diffusion processes of C_T through the pycnocline increased its surface concentration by an average of 3.55 ± 2.69 mmol m^{-3} during the entire annual cycle throughout the region. The vertical entrainment increased the surface C_T by an average of 0.58 ± 0.52 mmol m^{-3} between August and January and was canceled between February and July due to the elevation of the mixed layer and subsequent increase in stratification. About 5.7–5.8% of the seasonal change in NC_T at S1 (**Figure 4C**) was explained by vertical mixing processes. The vertical mixing inversely affected the change of NC_T at S3 and S5. During the periods of increase in NC_T, between 0.02 and 9.10% of the NC_T was removed from the surface by vertical mixing processes, while during periods of depletion, between 2.90 and 8.20% of the surface NC_T was injected from deep waters. The contribution of vertical transport was maximum in the northern part of S2 (∼29.7–36.7%) and at S4 (∼10.3–11.9%) (**Figures 4B,D**) due to the effect of internal waves in CS (Bruno et al., 2002; Macias et al., 2006) and the elevation of the pycnocline in the most Mediterranean part (Echevarría et al., 2002). The influence of the seasonality of the wind-induced upwelling on the change of NC_T by vertical mixing was detected in S2, where a difference of 1.34 mmol m^{-3} between increase and depletion periods was found.

The horizontal transport in the west-to-east direction decreased the surface NC_T (0.8–15.6%) in the entire annual cycle due to the lower A_T and C_T content of the Atlantic inflow compared to the Mediterranean outflow (de la Paz et al., 2008). An increase in NC_T by horizontal transport was only observed at S1 (0.4%) and in the northern part of S4 (2.6%) and S5 (9.6%).

The average seasonal change of NC_T for all selected locations across the Strait of Gibraltar was 29.0 ± 9.96 mmol m^{-3}. Biological processes controlled the seasonal change of surface NC_T (93.5–95.6%), increasing its concentration by 27.72 mmol m^{-3} in periods of higher remineralization influence and decreasing it by 27.11 mmol m^{-3} when production was the controlling process. The contribution of air-sea CO_2 exchange (0.9–3.3%) was higher during the increasing periods due to the strong behavior as a sink of the channel (0.94 and 0.27 mmol m^{-3} during the increase and depletion periods, respectively). Vertical mixing increased the NC_T by 1.32 mmol m^{-3} and decreased it by 1.02 mmol m^{-3}, with a total contribution of 4.1%. Finally, the effect of horizontal transport was minimal (<2.8%) and decreased the NC_T by 1.08 and 0.52 mmol m^{-3} in both total increase and depletion periods, respectively.

CO_2 Fluxes in the Strait of Gibraltar

The temporal distribution of FCO_2 calculated from observed and computed data allowed the characterization of the air-sea CO_2 exchange in the Strait of Gibraltar throughout the study period. The monthly average FCO_2 values (**Supplementary Figure 8**) proved the strong behavior of the region as a CO_2 sink from November to July and as a weak source between August and October. This seasonal pattern is consistent with previous studies in the Strait of Gibraltar (de la Paz et al., 2009, 2011) and along the coastal to open-ocean transitional area of the Northeast Atlantic (Curbelo-Hernández et al., 2021). In the northern section, the CO_2 sink behavior remained throughout the first year of observation (February 2019–February 2020) even in the warm months, while a late-summer CO_2 source behavior was found in the second year of observation (March 2020–March 2021). In contrast, the southern section behaved as a late-summer CO_2 source in both entire years considered.

The FCO_2 values show a direct relationship with ΔfCO_2 in both the northern and the southern sections [0.11 (r^2 = 0.87 and ρ = 0.93) and 0.14 (r^2 = 0.72 and ρ = 0.84) mmol m^{-2} d^{-1} μatm^{-1}, respectively]. Despite the important role of the wind speed and direction controlling the seasonal and spatial distribution and intensity of upwelling events across coastal areas in the Strait of Gibraltar (Stanichny et al., 2005), its short-term variability is not significant on an annual time scale in this region (de la Paz et al., 2011) and specially along the northern section. The difference between the averages FCO_2 calculated with satellite and measured wind speed data was 0.14 mol C m^{-2} $year^{-1}$. The changes in wind speed influence the intensity of CO_2 exchange between low atmosphere and surface ocean and could modified the physical properties of the upper layers, but do not determine the formation of CO_2 source/sink. Northeasterly winds bring on the deep-water injection in upper layers and subsequent cooling of the surface seawater in the southwest area, favoring the solubility of atmospheric CO_2. Accordingly, a more intense annual CO_2 sink was found in this area compared to the northwest area (**Figure 5**). The assessment of the spatio-temporal changes of FCO_2 in this study show that the formation of the seasonal CO_2 sink and source is controlled by the ΔfCO_2 variations influenced by changes in the physical properties of the surface ocean, which were driven by the local climatology and the unique hydrology of the channel (**Supplementary Figure 8**). Therefore, Eq. 16 which provides $fCO_{2,sw}$ data for the area using SST as unknown

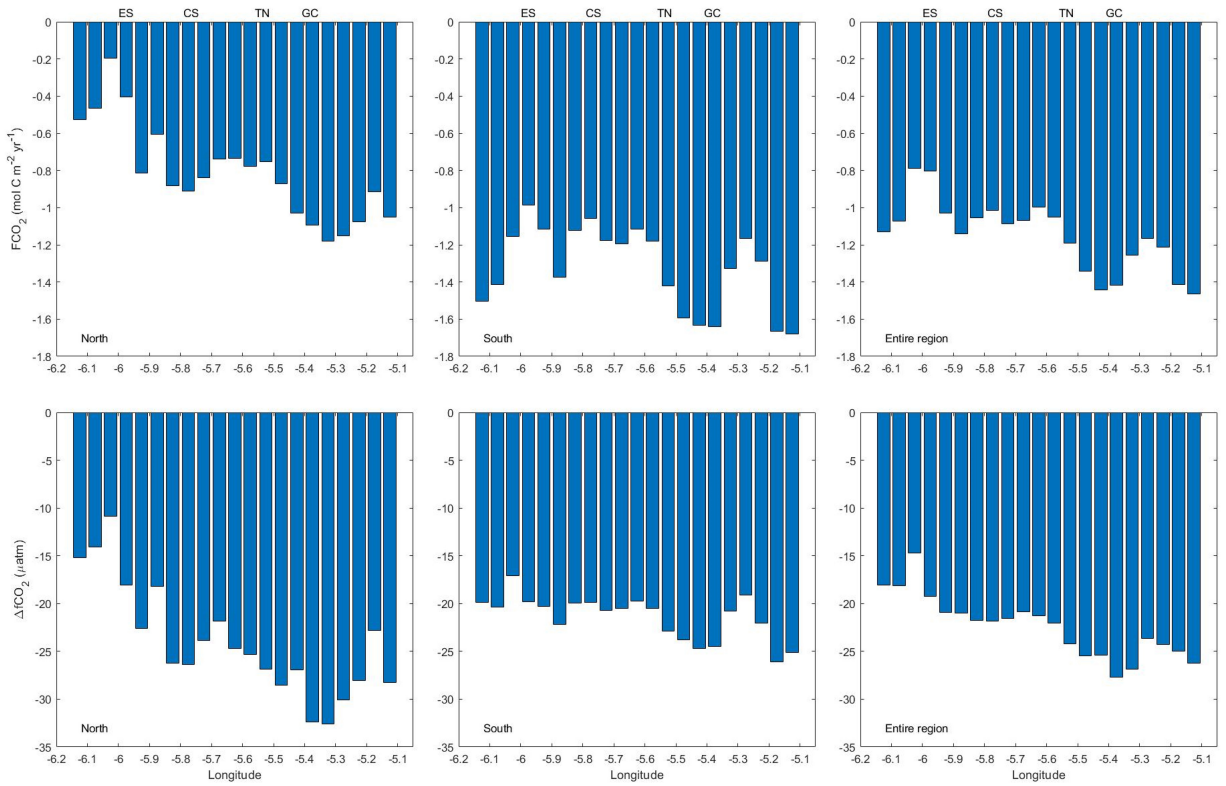

FIGURE 5 | Annual average of FCO_2 and ΔfCO_2 every 0.05° longitude calculated along the northern and southern sections and in the entire region.

variable (available from satellite data) together with satellite winds, can be used to estimate long term CO_2 fluxes in the Strait of Gibraltar.

The annual negative values of FCO_2 obtained along both the northern and the southern section show that the Strait of Gibraltar behaved as a net CO_2 sink (**Figure 5**). The annual average FCO_2, ΔfCO_2, and wind speed were calculated at all the selected stations, along the northern and southern sections and in the entire region (**Table 4**). The average ingassing was found to be maximum in the eastern area (**Figure 5**). The total annual FCO_2 in most of the Northeast Atlantic and Mediterranean Sea parts of the channel was −1.02 and −1.30 mol C m^{-2} $year^{-1}$, respectively, which is related with lower SST values observed throughout the year and the enhancement of the biological uptake toward the northeastern part of the channel (Echevarría et al., 2002) that increased the ΔfCO_2.

The net CO_2 sink obtained in this study between 2019 and 2021 for the entire region was −0.98 mol C m^{-2} $year^{-1}$, which falls in the range of the first annual FCO_2 provided by Santana-Casiano et al. (2002) (−2.5 mol C m^{-2} $year^{-1}$) and the annual FCO_2 reported in most recent studies of de la Paz et al. (2009) (−0.28 mol C m^{-2} $year^{-1}$) and de la Paz et al. (2011) (-0.02 ± 0.13 mol C m^{-2} $year^{-1}$). The annual FCO_2 was calculated in these studies from limited datasets and using the parameterization of Wanninkhof (1992) (W92). When applying this parameterization to the data collected, an annual value of FCO_2 of −1.21 mol C m^{-2} $year^{-1}$ was obtained. This average ingassing is more than two times higher than the values reported with W92 for the Gulf of Cadiz (−0.4 mol C m^{-2} $year^{-1}$; Borges et al., 2006) and for the Northwest African Atlantic coast (−0.59 mol C m^{-2} $year^{-1}$, using W92; Curbelo-Hernández et al., 2021). However, it falls within the annual FCO_2 estimated by Chen et al. (2013) for the Northeast Atlantic (−1.04 mol C m^{-2} $year^{-1}$) and for the Iberian upwelling (−1.33 mol C m^{-2} $year^{-1}$). The net CO_2 sink reported in this study is consistent with that obtained from SOCAT data referenced to 2019 (−0.97 mol C m^{-2} $year^{-1}$; using W92).

The net FCO_2 for the entire area (1650 km^2) was −7.12 Gg CO_2 $year^{-1}$ (1 Gg = 10^9 g) (−1.94 Gg C $year^{-1}$). This result is in agreement with previous studies of the behavior of the coastal regions and continental shelves as a net CO_2 sink (e.g., Borges et al., 2006, 2005; Chen and Borges, 2009; Laruelle et al., 2010, 2013, 2018; Cai et al., 2006; Cai, 2011; Chen et al., 2013) and can be integrated into the estimated net CO_2 sink for the European coastal regions (-68.1×10^3 Gg C $year^{-1}$; Borges et al., 2006) and global continental shelves (-0.4×10^6 Gg C $year^{-1}$; Chen et al., 2013).

CONCLUSION

The spatio-temporal variability of the CO_2 system and fluxes in the Strait of Gibraltar was assessed with a high-resolution dataset in this study. The results obtained between February 2019 and

TABLE 4 | Annual average FCO_2, ΔfCO_2, and wind speed obtained during the first and second year of observation (February 2019–February 2020 and March 2020–March 2021, respectively) and throughout the study period at stations S1–S5, along the northern and southern sections and in the entire region.

			February 2019–February 2020		March 2020–March 2021		February 2019–March 2021	
			Mean	Standard deviation	Mean	Standard deviation	Mean	Standard deviation
FCO_2 (mol C m^{-2} $year^{-1}$)	S1		−0.90	0.93	−0.81	1.12	−0.86	1.03
	S2	North	−1.03	0.66	−0.89	0.92	−0.96	0.80
		South	−0.87	0.78	−0.69	1.02	−0.78	0.91
	S3	North	−1.12	0.64	−0.93	0.90	−1.03	0.79
		South	−0.95	0.60	−0.78	1.00	−0.87	0.83
	S4	North	−1.48	0.51	−1.02	0.68	−1.25	0.65
		South	−1.11	0.75	−0.83	0.96	−0.97	0.87
	S5	North	−1.59	0.33	−0.71	0.67	−1.15	0.69
		South	−1.16	0.57	−1.03	0.86	−1.10	0.73
	Section	North	−1.03	0.69	−0.66	0.81	−0.82	0.78
		South	−0.89	0.85	−1.12	1.15	−1.01	1.02
	Entire region		−1.03	0.87	−0.93	1.01	−0.98	0.94
ΔfCO_2 (μatm)	S1		−15.80	16.82	−14.72	22.27	−15.25	19.74
	S2	North	−19.98	9.55	−19.28	21.03	−19.63	16.34
		South	−16.76	13.40	−14.31	21.12	−15.53	17.73
	S3	North	−21.66	9.43	−21.58	20.83	−21.62	16.17
		South	−18.86	8.67	−15.11	20.86	−16.98	16.09
	S4	North	−27.31	6.37	−25.61	17.14	−26.46	12.96
		South	−21.44	9.28	−19.24	22.02	−20.34	16.94
	S5	North	−34.57	9.41	−25.82	22.05	−30.19	17.51
		South	−21.57	8.11	−23.58	18.84	−22.58	14.54
	Section	North	−34.42	23.22	−22.10	22.02	−28.24	23.44
		South	−15.80	13.96	−14.60	19.44	−15.20	16.93
	Entire region		−18.39	13.30	−18.29	20.78	−18.34	17.44
Wind speed (m s^{-1})	S1		8.15	1.31	8.47	1.17	8.31	1.25
	S2	North	8.06	1.16	8.06	1.13	8.06	1.14
		South	8.25	1.27	8.23	1.22	8.24	1.24
	S3	North	8.05	1.06	7.87	1.30	7.96	1.19
		South	8.09	1.25	8.32	0.73	8.20	1.03
	S4	North	8.52	0.78	7.70	1.43	8.11	1.22
		South	7.86	1.36	7.92	1.34	7.89	1.35
	S5	North	8.14	1.20	6.83	1.68	7.48	1.60
		South	8.41	0.95	7.88	1.46	8.15	1.26
	Section	North	8.25	1.40	6.97	0.90	7.61	1.34
		South	8.08	1.72	9.33	1.88	8.71	1.91
	Entire region		8.27	1.48	8.32	1.53	8.29	1.50

March 2021 provided the seasonal and spatial variability of the surface CO_2. Although seasonal temperature fluctuation was the main driver of the observed changes in the CO_2 system in this region, the temporal and spatial distribution of the variables was strongly influenced by physical and biological factors oscillations due to the seasonal change in the depth of the AMI layer, the wind-induced upwelling during northeasterly winds and the tidal-induced pulsating upwelling throughout the year and especially during spring tides. The elevation of the AMI layer toward the northeast and the wind-induced upwelling on the African coast toward the west of TN favors the vertical mixing and enhances the physical–biological coupling in the northeast and southwest part of the channel. In these areas of lower SST and higher SSS, the change in $fCO_{2,sw}$ with temperature was lower due to the increase in the importance of the non-thermal effects. The annual cycle of surface $fCO_{2,sw}$ was described in this study (Eqs 14, 15) by considering the seasonality of SST and its spatial changes controlled by the local climatology and the unique hydrology of the channel. Equation 16 allows to compute past, present, and future surface $fCO_{2,sw}$ values using satellite SST values. The $fCO_{2,sw}$ was found to increase with temperature by 9.02 ± 1.99 μatm °C (r^2 = 0.86 and ρ = 0.93) and 4.51 ± 1.66 μatm °C (r^2 = 0.48 and ρ = 0.69) in the northern and southern sections, respectively.

The seasonality of NC_T was mainly controlled by NCP processes (93.5–95.6%), while the contribution of air-sea

exchange (0.9–3.3%), horizontal transport (1.8–3.7%), and vertical mixing (3.5–4.6%) was minimal. The seasonality of NC_T was higher in the region most influenced by wind-induced upwelling to the southwest of the channel (42.65 and 45.44 mmol m^{-3} calculated in the southern part of S2 and S3, respectively). In the areas of maximum upwelling, the contribution of NCP compared to that of air-sea exchange was found to be maximum (>81.0 and <13.1%, respectively).

In terms of air-sea CO_2 exchange, the Strait of Gibraltar behaved as a strong CO_2 sink during the cold months (between −7 and −2 mmol m^{-2} $year^{-1}$) and as a weak source during the warm months (<3 mmol m^{-2} $year^{-1}$). Considering the high variability in the CO_2 sink and integrating the entire area (6.1–5.1°W, 1650 km^2) an average CO_2 flux of −7.12 Gg CO_2 $year^{-1}$ (−1.94 Gg C $year^{-1}$) was determined. The net CO_2 sink was higher toward the east of TN (−1.30 mol C m^{-2} $year^{-1}$), where the depth of the AMI layer is minimum and both solubility and biological uptake were enhanced by the injection of deep, cold, and nutrient-rich water throughout the year. The net CO_2 sink weakened toward the west of TN (−1.02 mol C m^{-2} $year^{-1}$), where higher annual SST values were obtained due to vertical mixing processes are limited to periods of wind-induced upwelling.

The present study shows that VOS lines are a powerful tool to study the carbon cycle in global and regional surface ocean. The continuous monitoring of the surface CO_2 by VOS lines is especially important in poorly known and highly variable areas such as the Strait of Gibraltar, where the observational data from oceanographic surveys are limited and continuous monitoring through other observational strategies is difficult to perform due to maritime traffic and socio-political factors. We provide in this study clear evidence of the complex processes related to the unique hydrology and local climatology of the transition region of the Strait of Gibraltar involved in the surface distribution of the CO_2 system variables. The air-sea CO_2 exchange and the surface inorganic carbon concentration, as well as the processes that control them, were assessed and quantified with an improved degree of certainty. These findings enhance the understanding of the surface CO_2 system and air-sea exchange in marginal and semi-enclosed seas and can be used to further compute how much of this atmospheric CO_2 entering in the surface ocean is finally transported into the ocean interior.

DATA AVAILABILITY STATEMENT

The datasets presented in this study can be found in online repositories. The names of the repository/repositories and accession number(s) can be found below: https://www.socat.info/.

AUTHOR CONTRIBUTIONS

MG-D, JMS-C, and AGG installed and maintained the equipment in the VOS line. DC-H performed the data treatments and MATLAB® routines. All authors made significant contributions toward the writing of the manuscript.

FUNDING

This study was supported by the Canary Islands Government and the Loro Parque Foundation through the CanBIO project, CanOA subproject (2019–2022), and the CARBOCAN agreement (Consejería de Transición Ecológica, Lucha contra el Cambio Climático y Planificación Territorial, and Gobierno de Canarias).

ACKNOWLEDGMENTS

We would like to thank the RENATE P ship owner, the NISA-Marítima company and the captains and crew members for the support during this collaboration. Special thanks to the technician Adrian Castro-Alamo for biweekly equipment maintenance and discrete sampling of total alkalinity aboard the ship. We thank the editor and reviewers for their constructive comments and suggestions, which helped to improve the quality of the manuscript. The VOS line will be part of the Spanish contribution to the Integrated Carbon Observation System (ICOS), European Research Infrastructure starting in 2021. We also thank the Surface Ocean CO_2 Atlas (SOCAT), an international effort, endorsed by the International Ocean Carbon Coordination Project (IOCCP), the Surface Ocean Lower Atmosphere Study (SOLAS), and the Integrated Marine Biosphere Research (IMBeR) program, to deliver a uniformly quality-controlled surface ocean CO_2 database. The many researchers and funding agencies responsible for the collection of data and quality control are thanked for their contributions to SOCAT.

SUPPLEMENTARY MATERIAL

The Supplementary Material for this article can be found online at: https://www.frontiersin.org/articles/10.3389/fmars.2021.745304/full#supplementary-material

REFERENCES

Allen, R. G., Pereira, L. S., Raes, D., and Smith, M. (1998). *Crop Evapotranspiration -Guidelines for Computing Crop Water Requirements*. FAO Irrigation and Drainage Paper 56. Rome: Food and Agriculture Organization.

Alonso del Rosario, J. J., Mejías, M. B., and Vázquez-Escobar, A. (2003). The influence of tidal hydrodynamic conditions on the generation of lee waves at the main sill of the Strait of Gibraltar. *Deep Sea Res. 1 Oceanogr. Res. Pap.* 50, 1005–1021. doi: 10.1016/S0967-0637(03)00097-9

Armi, L., and Farmer, D. M. (1988). The flow of Mediterranean water through the Strait of Gibraltar. the flow of Atlantic water through the Strait of Gibraltar. *Prog. Oceanogr.* 21, 1–105.

Bates, N. R., Astor, Y. M., Church, M. J., Currie, K., Dore, J. E., González-Dávila, M., et al. (2014). A time-series view of changing surface ocean chemistry due to ocean uptake of anthropogenic CO2 and ocean acidification. *Oceanography* 27, 126–141. doi: 10.5670/oceanog.2014.16

Bégovic, M., and Copin-Montégut, C. (2002). Processes controlling annual variations in the partial pressure of CO2 in surface waters of the central northwestern Mediterranean Sea (Dyfamed site). *Deep Sea Res. 2 Top. Stud. Oceanogr.* 49, 2031–2047. doi: 10.1016/S0967-0645(02)00026-7

Bolado-Penagos, M., González, C. J., Chioua, J., Sala, I., Gomiz-Pascual, J. J., Vázquez-Escobar, A., et al. (2020). Submesoscale processes in the coastal margins of the Strait of Gibraltar. The Trafalgar–Alboran connection. *Prog. Oceanogr.* 181:102219. doi: 10.1016/j.pocean.2019.102219

Borges, A. V., Delille, B., and Frankignoulle, M. (2005). Budgeting sinks and sources of CO2 in the coastal ocean: diversity of ecosystem counts. *Geophys. Res. Lett.* 32, 1–4. doi: 10.1029/2005GL023053

Borges, A. V., Schiettecatte, L. S., Abril, G., Delille, B., and Gazeau, F. (2006). Carbon dioxide in European coastal waters. *Estuar. Coast. Shelf Sci.* 70, 375–387. doi: 10.1016/j.ecss.2006.05.046

Boyce, F. M. (1975). Internal waves in the Straits of Gibraltar. *Deep. Res. Oceanogr. Abstr.* 22, 597–610. doi: 10.1016/0011-7471(75)90047-9

Bray, N. A., Ochoa, J., and Kinder, T. H. (1995). The role of the interface in exchange through the Strait of Gibraltar. *J. Geophys. Res.* 100, 10755–10776. doi: 10.1029/95JC00381

Broecker, W. S., and Peng, T. H. (1982). *Tracers in the Sea*. Palisades, NY: Eldigio Press, 1–690.

Bruno, M., Alonso, J. J., Cózar, A., Vidal, J., Ruiz-Cañavate, A., Echevarría, F., et al. (2002). The boiling-water phenomena at Camarinal Sill, the Strait of Gibraltar. *Deep. Sea Res. 2 Top. Stud. Oceanogr.* 49, 4097–4113. doi: 10.1016/S0967-0645(02)00144-3

Bryden, H. L., Candela, J., and Kinder, T. H. (1994). Exchange through the Strait of Gibraltar. *Prog. Oceanogr.* 33, 201–248. doi: 10.1016/0079-6611(94)90028-0

Bryden, H. L., and Kinder, T. H. (1991). Steady two-layer exchange through the Strait of Gibraltar. *Deep Sea Res. A Oceanogr. Res. Pap.* 38, S445–S463. doi: 10.1016/s0198-0149(12)80020-3

Cai, W. J. (2011). Estuarine and coastal ocean carbon paradox: CO_2 sinks or sites of terrestrial carbon incineration? *Ann. Rev. Mar. Sci.* 3, 123–145. doi: 10.1146/annurev-marine-120709-142723

Cai, W. J., Dai, M., and Wang, Y. (2006). Air-sea exchange of carbon dioxide in ocean margins: a province-based synthesis. *Geophys. Res. Lett.* 33:L12603. doi: 10.1029/2006GL026219

Candela, J., Winant, C., and Ruiz, A. (1990). Tides in the Strait of Gibraltar. *J. Geophys. Res.* 95, 7313–7335. doi: 10.1029/JC095iC05p07313

Candela, J., Winant, C. D., and Bryden, H. L. (1989). Meteorologically forced subinertial flows through the Strait of Gibraltar. *J. Geophys. Res. Ocean.* 94, 12667–12679. doi: 10.1029/JC094iC09p12667

Chen, C. T. A., and Borges, A. V. (2009). Reconciling opposing views on carbon cycling in the coastal ocean: continental shelves as sinks and near-shore ecosystems as sources of atmospheric CO2. *Deep. Sea Res. 2: Top. Stud. Oceanogr.* 56, 578–590. doi: 10.1016/j.dsr2.2009.01.001

Chen, C. T. A., Huang, T. H., Chen, Y. C., Bai, Y., He, X., and Kang, Y. (2013). Air-sea exchanges of coin the world's coastal seas. *Biogeosciences* 10, 6509–6544. doi: 10.5194/bg-10-6509-2013

Chen, C. T. A., and Pytkowicz, R. M. (1979). On the total CO2-titration alkalinity-Oxygen system in the Pacific Ocean [5]. *Nature* 281, 362–365. doi: 10.1038/281362a0

Curbelo-Hernández, D., González-Dávila, M., González, A. G., González-Santana, D., and Santana-Casiano, J. M. (2021). CO2 fluxes in the Northeast Atlantic Ocean based on measurements from a surface ocean observation platform. *Sci. Total Environ.* 775:145804. doi: 10.1016/j.scitotenv.2021.145804

Dafner, E., González-Dávila, M., Santana-Casiano, J. M., and Sempéré, R. (2001). Total organic and inorganic carbon exchange through the Strait of Gibraltar in September 1997. *Deep Sea Res. 1 Oceanogr. Res. Pap.* 48, 1217–1235. doi: 10.1016/S0967-0637(00)00064-9

de la Paz, M., Debelius, B., Macías, D., Vázquez-Escobar, A., Gómez-Parra, A., and Forja, J. M. (2008). Tidal-induced inorganic carbon dynamics in the Strait of Gibraltar. *Cont. Shelf Res.* 28, 1827–1837. doi: 10.1016/j.csr.2008.04.012

de la Paz, M., Gómez-Parra, A., and Forja, J. (2009). Seasonal variability of surface fCO2 in the Strait of Gibraltar. *Aquat. Sci.* 71, 55–64. doi: 10.1007/s00027-008-8060-y

de la Paz, M., Huertas, E. M., Padín, X. A., Gónzalez-Dávila, M., Santana-Casiano, J. M., Forja, J. M., et al. (2011). Reconstruction of the seasonal cycle of air-sea CO2 fluxes in the Strait of Gibraltar. *Mar. Chem.* 126, 155–162. doi: 10.1016/j.marchem.2011.05.004

Denman, K. L., and Gargett, A. E. (1983). Time and space scales of vertical mixing and advection of phytoplankton in the upper ocean. *Limnol. Oceanogr.* 28, 801–815.

Dickson, A. G. (1990). Standard potential of the reaction: AgCl(s) + 1 2H2(g) = Ag(s) + HCl(aq), and the standard acidity constant of the ion HSO4- in synthetic sea water from 273.15 to 318.15 K. *J. Chem. Thermodyn.* 22, 113–127. doi: 10.1016/0021-9614(90)90074-Z

Dickson, A. G., Sabine, C. L., and Chistian, J. R. (2007). Guide to best practices for ocean CO2 measurements. *PICES Special Publ.* 3:191.

Echevarría, F., García-Lafuente, J., Bruno, M., Gorsky, G., Goutx, M., González, N., et al. (2002). Physical-biological coupling in the Strait of Gibraltar. *Deep Sea Res. 2 Top. Stud. Oceanogr.* 49, 4115–4130. doi: 10.1016/S0967-0645(02)00145-5

Fasham, M. J. R., Ducklow, H. W., and McKelvie, S. M. (1990). A nitrogen-based model of plankton dynamics in the oceanic mixed layer. *J. Mar. Res.* 48, 591–639. doi: 10.1357/002224090784984678

Flecha, S., Pérez, F. F., Murata, A., Makaoui, A., and Huertas, I. E. (2019). Decadal acidification in Atlantic and Mediterranean water masses exchanging at the Strait of Gibraltar. *Sci. Rep.* 9:15533. doi: 10.1038/s41598-019-52084-x

Folkard, A. M., Davies, P. A., Fiúza, A. F. G., and Ambar, I. (1997). Remotely sensed sea surface thermal patterns in the Gulf of Cadiz and the Strait of Gibraltar: variability, correlations and relationships with the surface wind field. *J. Geophys. Res. Ocean.* 102, 5669–5683. doi: 10.1029/96JC02505

Frankignoulle, M., and Borges, A. V. (2001). European continental shelf as a significant sink for atmospheric carbon dioxide. *Glob. Biogeochem. Cycles* 15, 569–576. doi: 10.1029/2000GB001307

García-Lafuente, J., Sánchez-Román, A., Naranjo, C., and Sánchez-Garrido, J. C. (2011). The very first transformation of the Mediterranean outflow in the Strait of Gibraltar. *J. Geophys. Res. Ocean.* 116:7010. doi: 10.1029/2011JC006967

García-Lafuente, J., Vargas, J. M., Plaza, F., Sarhan, T., Candela, J., and Bascheck, B. (2000). Tide at the eastern section of the Strait of Gibraltar. *J. Geophys. Res. Ocean.* 105, 14197–14213. doi: 10.1029/2000jc900007

Gascard, J. C., and Richez, C. (1985). Water masses and circulation in the Western Alboran Sea and in the Strait of Gibraltar. *Prog. Oceanogr.* 15, 157–216. doi: 10.1016/0079-6611(85)90031-X

Gómez, F., Echevarría, F., García, C. M., Prieto, L., Ruiz, J., Reul, A., et al. (2000). Microplankton distribution in the Strait of Gibraltar: coupling between organisms and hydrodynamic structures. *J. Plankton Res.* 22, 603–617. doi: 10.1093/plankt/22.4.603

Gómez, F., Gorsky, G., Striby, L., Vargas, J. M., Gonzalez, N., Picheral, M., et al. (2001). Small-scale temporal variations in biogeochemical features in the Strait of Gibraltar, Mediterranean side–the role of NACW and the interface oscillation. *J. Mar. Syst.* 30, 207–220. doi: 10.1016/S0924-7963(01)00059-8

Gómez-Jakobsen, F. J., Mercado, J. M., Cortés, D., Yebra, L., and Salles, S. (2019). A first description of the summer upwelling off the Bay of Algeciras and its role in the northwestern Alboran Sea. *Estuar. Coast. Shelf Sci.* 225:106230. doi: 10.1016/j.ecss.2019.05.012

González-Dávila, M., Santana-Casiano, J. M., Rueda, M. J., Llinás, O., and González-Dávila, E. F. (2003). Seasonal and interannual variability of sea-surface carbon dioxide species at the European Station for Time Series in the Ocean at the Canary Islands (ESTOC) between 1996 and 2000. *Glob. Biogeochem. Cycles* 17:1076. doi: 10.1029/2002gb001993

Gruber, N., Keeling, C. D., and Stocker, T. F. (1998). Carbon-13 constraints on the seasonal inorganic carbon budget at the BATS site in the northwestern Sargasso Sea. *Deep Sea Res. 1 Oceanogr. Res. Pap.* 45, 673–717. doi: 10.1016/S0967-0637(97)00098-8

Huertas, I. E., Ríos, A. F., García-Lafuente, J., Makaoui, A., Rodríguez-Gálvez, S., Sánchez-Román, A., et al. (2009). Anthropogenic and natural CO2 exchange through the Strait of Gibraltar. *Biogeosciences* 6, 647–662. doi: 10.5194/bg-6-647-2009

IPCC (2007). *Climate Change 2007: The Physical Science Basis*. Contribution of Working Group I to the Fourth Assessment Report of the Intergovernmental Panel on Climate Change, eds S. Solomon, D. Qin, M. Manning, Z. Chen, M. Marquis, K. B. Averyt, et al. Cambridge: Cambridge University Press.

IPCC (2021). *Climate Change 2021: The Physical Science Basis*. Contribution of Working Group I to the Sixth Assessment Report of the Intergovernmental Panel on Climate Change, eds V. Masson-Delmotte, P. Zhai, A. Pirani, S. L. Connors, C. Péan, S. Berger, et al. Cambridge: Cambridge University Press.

La Violette, P. E., and Arnone, R. A. (1988). A tide-generated internal waveform in the western approaches to the Strait of Gibraltar. *J. Geophys. Res. Ocean.* 93, 15653–15667. doi: 10.1029/JC093iC12p15653

Lacombe, H., and Richez, C. (1982). The regime of the Strait of Gibraltar. *Oceanogr. Ser.* 34, 13–73. doi: 10.1016/S0422-9894(08)71237-6

Laruelle, G. G., Cai, W. J., Hu, X., Gruber, N., Mackenzie, F. T., and Regnier, P. (2018). Continental shelves as a variable but increasing global sink for atmospheric carbon dioxide. *Nat. Commun.* 9:454. doi: 10.1038/s41467-017-02738-z

Laruelle, G. G., Dürr, H. H., Lauerwald, R., Hartmann, J., Slomp, C. P., Goossens, N., et al. (2013). Global multi-scale segmentation of continental and coastal waters from the watersheds to the continental margins. *Hydrol. Earth Syst. Sci.* 17, 2029–2051. doi: 10.5194/hess-17-2029-2013

Laruelle, G. G., Dürr, H. H., Slomp, C. P., and Borges, A. V. (2010). Evaluation of sinks and sources of CO2 in the global coastal ocean using a spatially-explicit typology of estuaries and continental shelves. *Geophys. Res. Lett.* 37:L15607. doi: 10.1029/2010GL043691

Lee, K., Kim, T. W., Byrne, R. H., Millero, F. J., Feely, R. A., and Liu, Y. M. (2010). The universal ratio of boron to chlorinity for the North Pacific and North Atlantic oceans. *Geochim. Cosmochim.* 74, 1801–1811. doi: 10.1016/j.gca.2009.12.027

Lee, K., Tong, L. T., Millero, F. J., Sabine, C. L., Dickson, A. G., Goyet, C., et al. (2006). Global relationships of total alkalinity with salinity and temperature in surface waters of the world's oceans. *Geophys. Res. Lett.* 33, 1–5. doi: 10.1029/2006GL027207

Lee, K., Wanninkhof, R., Feely, R. A., Millero, F. J., and Peng, T. H. (2000). Global relationships of total inorganic carbon with temperature and nitrate in surface seawater. *Glob. Biogeochem. Cycles* 14, 979–994. doi: 10.1029/1998GB001087

Lueker, T. J., Dickson, A. G., and Keeling, C. D. (2000). Ocean pCO2 calculated from dissolved inorganic carbon, alkalinity, and equations for K1 and K2: validation based on laboratory measurements of CO2 in gas and seawater at equilibrium. *Mar. Chem.* 70, 105–119. doi: 10.1016/S0304-4203(00)00022-0

Lüger, H., Wallace, D. W. R., Körtzinger, A., and Nojiri, Y. (2004). The pCO2 variability in the midlatitude North Atlantic Ocean during a full annual cycle. *Glob. Biogeochem. Cycles* 18:GB3023. doi: 10.1029/2003GB002200

Macias, D., García, C. M., Echevarría, F., Vázquez-Escobar, A., and Mejías, M. B. (2006). Tidal induced variability of mixing processes on Camarinal Sill (Strait of Gibraltar): a pulsating event. *J. Mar. Syst.* 60, 177–192. doi: 10.1016/j.jmarsys.2005.12.003

Macías, D., Martin, A. P., García-Lafuente, J., García, C. M., Yool, A., Bruno, M., et al. (2007). Analysis of mixing and biogeochemical effects induced by tides on the Atlantic-Mediterranean flow in the Strait of Gibraltar through a physical-biological coupled model. *Prog. Oceanogr.* 74, 252–272. doi: 10.1016/j.pocean.2007.04.006

Mackenzie, F. T., Lerman, A., and Ver, L. M. B. (1998). Role of the continental margin in the global carbon balance during the past three centuries. *Geology* 26, 423–426. doi: 10.1130/0091-76131998026<0423:ROTCMI<2.3.CO;2

Minas, H. J., Coste, B., Le Corre, P., Minas, M., and Raimbault, P. (1991). Biological and geochemical signatures associated with the water circulation through the Strait of Gibraltar and in the western Alboran Sea. *J. Geophys. Res.* 96, 8755–8771. doi: 10.1029/91JC00360

Mintrop, L., Pérez, F. F., González-Dávila, M., Santana-Casiano, J. M., and Körtzinger, A. (2000). Alkalinity determination by potentiometry: intercalibration using three different methods. *Ciencias Mar.* 26, 23–37. doi: 10.7773/cm.v26i1.573

Muller-Karger, F. E., Varela, R., Thunell, R., Luerssen, R., Hu, C., and Walsh, J. J. (2005). The importance of continental margins in the global carbon cycle. *Geophys. Res. Lett.* 32, 1–4. doi: 10.1029/2004GL021346

Peliz, A., Teles-Machado, A., Marchesiello, P., Dubert, J., and García-Lafuente, J. (2009). Filament generation off the Strait of Gibraltar in response to Gap winds. *Dyn. Atmos. Ocean.* 46, 36–45. doi: 10.1016/j.dynatmoce.2008.08.002

Peng, T. H., Takahashi, T., Broecker, W. S., and Olafsson, J. (1987). Seasonal variability of carbon dioxide, nutrients and oxygen in the northern North Atlantic surface water: observations and a model. *Tellus B Chem. Phys. Meteorol.* 39, 439–458. doi: 10.3402/tellusb.v39i5.15361

Pierrot, D., Neill, C., Sullivan, K., Castle, R., Wanninkhof, R., Lüger, H., et al. (2009). Recommendations for autonomous underway pCO2 measuring systems and data-reduction routines. *Deep Sea Res. 2 Top. Stud. Oceanogr.* 56, 512–522. doi: 10.1016/j.dsr2.2008.12.005

Pistek, P., and La Violette, P. E. (1999). Observations of the suppression of tide-generated nonlinear internal wave packets in the Strait of Gibraltar. *J. Mar. Syst.* 20, 113–128. doi: 10.1016/S0924-7963(98)00073-6

Ramírez-Romero, E., Macías, D., García, C. M., and Bruno, M. (2014). Biogeochemical patterns in the Atlantic Inflow through the Strait of Gibraltar. *Deep Sea Res. 1 Oceanogr. Res. Pap.* 85, 88–100. doi: 10.1016/j.dsr.2013.12.004

Richez, C. (1994). Airborne synthetic aperture radar tracking of internal waves in the Strait of Gibraltar. *Prog. Oceanogr.* 33, 93–159. doi: 10.1016/0079-6611(94)90023-X

Richez, C., and Kergomard, C. (1990). "Characteristic features occurring in the Strait of Gibraltar as seen through remote sensing data," in *The Physical Oceanography of Sea Straits*, ed. L. J. Pratt (Dordrecht: Springer), 441–455. doi: 10.1007/978-94-009-0677-8_21

Sammartino, S., García-Lafuente, J., Naranjo, C., Sánchez-Garrido, J. C., Sánchez-Leal, R., and Sánchez-Román, A. (2015). Ten years of marine current measurements in Espartel Sill, Strait of Gibraltar. *J. Geophys. Res. Ocean.* 120, 6309–6328. doi: 10.1002/2014JC010674

Sánchez-Garrido, J. C., García-Lafuente, J., Criado-Aldeanueva, F., Baquerizo, A., and Sannino, G. (2008). Time-spatial variability observed in velocity of propagation of the internal bore in the Strait of Gibraltar. *J. Geophys. Res. Ocean.* 113, 1–6. doi: 10.1029/2007JC004624

Sánchez-Garrido, J. C., Sannino, G., Liberti, L., García-Lafuente, J., and Pratt, L. (2011). Numerical modeling of three-dimensional stratified tidal flow over Camarinal Sill, Strait of Gibraltar. *J. Geophys. Res. Ocean.* 116:12026. doi: 10.1029/2011JC007093

Santana-Casiano, J. M., Gonzalez-Davila, M., and Laglera, L. M. (2002). The carbon dioxide system in the Strait of Gibraltar. *Deep. Res. 2 Top. Stud. Oceanogr.* 49, 4145–4161. doi: 10.1016/S0967-0645(02)00147-9

Santana-Casiano, J. M., González-Dávila, M., Laglera-Baquer, L. M., and Rodriguez-Somoza, M. J. (2001). Carbon dioxide system in the Canary region during October 1995. *Sci. Mar.* 65, 41–49. doi: 10.3989/scimar.2001.65s141

Sarmiento, J. L., and Gruber, N. (2006). *Ocean Biogeochemical Dynamics. Geological Magazine*. Princeton: Princeton University Press, 144:1034. doi: 10.1017/S0016756807003755

Shadwick, E. H., Thomas, H., Azetsu-Scott, K., Greenan, B. J. W., Head, E., and Horne, E. (2011). Seasonal variability of dissolved inorganic carbon and surface water pCO2 in the Scotian Shelf region of the Northwestern Atlantic. *Mar. Chem.* 124, 23–37. doi: 10.1016/j.marchem.2010.11.004

Shadwick, E. H., Thomas, H., Comeau, A., Craig, S. E., Hunt, C. W., and Salisbury, J. E. (2010). Air-sea CO2 fluxes on the Scotian Shelf: seasonal to multi-annual variability. *Biogeosciences* 7, 3851–3867. doi: 10.5194/bg-7-3851-2010

Skliris, N., and Beckers, J. (2009). Modelling the Gibraltar Strait/Western Alboran Sea ecohydrodynamics. *Dtsch. Hydrographische Z.* 59, 489–508. doi: 10.1007/s10236-009-0185-6

Stanichny, S., Tigny, V., Stanichnaya, R., and Djenidi, S. (2005). Wind driven upwelling along the African coast of the Strait of Gibraltar. *Geophys. Res. Lett.* 32, 1–4. doi: 10.1029/2004GL021760

Takahashi, T., Sutherland, S. C., Sweeney, C., Poisson, A., Metzl, N., Tilbrook, B., et al. (2002). Global air-sea flux of CO_2 based on surface ocean pCO_2, and seasonal biological and temperature effects. *Deep. Res. Part II* 49, 1601–1622.

Takahashi, T., Olafsson, J., Goddard, J. G., Chipman, D. W., and Sutherland, S. C. (1993). Seasonal variation of CO2 and nutrients in the high-latitude surface oceans: a comparative study. *Glob. Biogeochem. Cycles* 7, 843–878. doi: 10.1029/93GB02263

Vázquez-Escobar, A., Bruno, M., Izquierdo, A., Macías, D., and Ruiz-Cañavate, A. (2008). Meteorologically forced subinertial flows and internal wave generation at the main sill of the Strait of Gibraltar. *Deep Sea Res. 2 Oceanogr. Res. Pap.* 55, 1277–1283. doi: 10.1016/j.dsr.2008.05.008

Walsh, J. J. (1991). Importance of continental margins in the marine biogeochemical cycling of carbon and nitrogen. *Nature* 350, 53–55. doi: 10.1038/350053a0

Wanninkhof, R. (1992). Relationship between wind speed and gas exchange over the ocean. *J. Geophys. Res.* 97, 7373–7382. doi: 10.1029/92JC00188

Wanninkhof, R. (2014). Relationship between wind speed and gas exchange over the ocean revisited. *Limnol. Oceanogr. Methods* 12, 351–362. doi: 10.4319/lom.2014.12.351

Wanninkhof, R., and Feely, R. A. (1998). fCO2 dynamics in the Atlantic, South Pacific and South Indian oceans. *Mar. Chem.* 60, 15–31. doi: 10.1016/S0304-4203(97)00088-1

Watson, G., and Robinson, S. (1990). A study of internal waves propagation in the Strait of Gibraltar using shore-based marine radar images. *J. Phys. Oceanogr.* 20, 374–395. doi: 10.1175/1520-0485(1990)020<0374:ASOIWP>2.0.CO;2

Wesson, J. C., and Gregg, M. C. (1994). Mixing at camarinal sill in the Strait of Gibraltar. *J. Geophys. Res.* 99, 9847–9878. doi: 10.1029/94JC00256

Conflict of Interest: The authors declare that the research was conducted in the absence of any commercial or financial relationships that could be construed as a potential conflict of interest.

Publisher's Note: All claims expressed in this article are solely those of the authors and do not necessarily represent those of their affiliated organizations, or those of the publisher, the editors and the reviewers. Any product that may be evaluated in this article, or claim that may be made by its manufacturer, is not guaranteed or endorsed by the publisher.